Department of Environmental, Land and Infrastructure Engineering

Master of Science in Georesources and Geoenergy Engineering

Impact of Thermal Effect in Reservoir Dynamic Modelling

By

Dana Hamdan

S335265

Supervisors
Prof. Viberti Dario

Co-supervisor
Dr. Eloisa Salina Borello

Politecnico di Torino
June 18, 2026

Abstract

In a geothermal doublet consisting of one injection well and one production well, the cold water injected at the surface gradually displaces the hot reservoir fluid, creating an expanding thermal front whose geometry is controlled by the petrophysical properties of the reservoir, its geometry, and the well configuration.

Monitoring the spatial extent evolution of the cold front through periodic well tests at the injector provides significant information for optimized reservoir management.

To test the practical feasibility of this monitoring approach, synthetic pressure data were generated with the commercial numerical simulator tNavigator® (*tNavigator® Technical Reference Manual*, 2024). Two modelling approaches that account for temperature effects are available within that platform and were compared in this work: the Temperature option (TEMP), which works within a black-oil fluid model and treats water viscosity as a function of temperature through PVT tables, and the Compositional Thermal model (THERMAL), which computes all fluid properties using an equation of state (GERG-2008 in this work). Both formulations are used routinely in industry, yet to the author's knowledge their quantitative disagreements specifically with geothermal applications have not been systematically examined.

This thesis compares the thermal front predictions of Temperature and Compositional Thermal models applied to a simplified geothermal doublet geometry. Two thermodynamic cases are studied. The first is a low-enthalpy, liquid-dominated reservoir at 100 bara and 92°C, while the second is a high-enthalpy, vapor-dominated reservoir at 10 bara and 181°C, inspired by the Larderello-Travale field of southern Tuscany, Italy. In both cases, injected water was at 20°C. After a preliminary period of doublet operations, allowing the development of a significant cooled zone around the injector, a well test is simulated at the injector well, imposing 12h of production and 12 h of buildup. The resulting pressure transients are analyzed and matched using a radial composite model into Saphir NL (KAPPA Engineering), part of the KAPPA-Workstation software suite. Such model allows to approximate the cold-water thermal bank around the injector as the inner zone, characterized by high viscosity, surrounded by the undisturbed warm outer reservoir, characterized by a mobility contrast due to the lower viscosity. The composite inner radius and mobility ratio recovered from Kappa are then compared directly against the thermal front geometry computed by tNavigator®, allowing the accuracy of the well test to be assessed as a cold front monitoring tool. Furthermore, the thermal front obtained from the two thermal formulations are compared to determine whether the simpler Temperature model

can give a reliable estimate of the cold front behavior in the low enthalpy and/or high enthalpy scenario.

Crucial for the comparability of the results was the adoption of identical viscosity–temperature function in the two approaches. To this end, a WATVISCT table driven from NIST IAPWS-97 was imposed in the TEMP model.

In the low-enthalpy scenario, the derivative of the pressure profile clearly shows a radial composite trend, with the two horizontal stabilizations coherent with the water viscosities of the cold and warm zone, respectively. Furthermore, the Kappa-extracted composite radii agree with the cold-front radii measured directly in tNavigator®, confirming that the radial composite well test correctly approximates the spatial extent of the cold-water bank when the inner zone viscosity is properly constrained to the injection temperature conditions. Even though one can expect the two solvers to give similar results in the low enthalpy scenario, where the reservoir fluid remains single-phase liquid during all the simulation, results showed an appreciable difference in the predicted thermal front extension (about 20% after 6 months). This is due to a combined effect of the different modelling of formation volume factors, density and compressibility in function of pressure and temperature.

In the vapor-dominated high enthalpy case, the Temperature model underestimates the cold front extent in comparison to the Compositional model. Therefore, a design performed with black-oil approach would predict later breakthrough than will actually occur. Furthermore, the derivative of the pressure response shows an unexpected behavior, for both numerical approaches. After a first stabilization, coherent with the cold zone viscosity, and a transition zone compatible with the observed cooled area, the derivative rises in an unexpected way, not compatible with a closed boundary response. Such behavior may arise from change of phases, high mobility and/or compressibility contrast. However, a deep analysis of the observed behavior was beyond the scope of the present study and therefore merits further investigation.

Because the Temperature model cannot handle steam condensation, latent-heat release, or phase-equilibrium dynamics, the Compositional Thermal model is a more physically sound basis for managing cold-front advance and breakthrough risk in high-enthalpy reservoirs. Importantly, however, the results also show that even in the simpler liquid-dominated case the choice of thermal formulation has a non-negligible influence on the predicted doublet thermal behavior.

These findings provide guidance for practitioners selecting simulation models for geothermal reservoir characterization and well test design.

Acknowledgements

Above all, I owe a great deal to my supervisor, Professor Dario Viberti, whose steady guidance and patience carried this work from its earliest sketches to its final form.

My co-supervisor, Dr. Eloisa Salina Borello, was equally invaluable — her technical insights, practical suggestions, and encouragement kept me on track through the more difficult stretches of the research.

I am also grateful to the faculty and staff of DIATI at Politecnico di Torino, who created the kind of intellectual environment where questions are taken seriously and curiosity is encouraged.

These past two years have been challenging. I managed to finish this master's program while my home country was going through war, and I was far away from my family. Living abroad during such uncertain times often meant balancing academic work with worry for the people I love, and all the things happening thousands of kilometers away. This experience has taught me how important it is to keep going after knowledge, even during difficult situations.

None of this would have meant anything without my parents and family. They carried me through every difficult moment from thousands of kilometers away, and their belief in me never faltered even when mine did. To my sister Batoul, my flower girl — you were present in every single stage of this journey in ways that words cannot fully capture.

I am also grateful to my friends, colleagues, and everyone I met during my time in Turin. Their support and shared experiences made these years both meaningful and memorable.

To everyone who played a part in this work, whether directly or from far away: thank you. This thesis marks the end of my master's program, but it also stands as a record of something more personal — two years of learning to keep going when the circumstances make that hard.

Table of Contents

List of Tables

List of Figures

Nomenclature

Acronyms and Abbreviations

SYMBOL	DESCRIPTION
PTA	Pressure Transient Analysis
BHP	Bottom Hole Pressure
DAS	Distributed Acoustic Sensing
DTS	Distributed Temperature Sensing
HPT	Harmonic Pulse Testing
LTE	Local Thermal Equilibrium
LTNE	Local Thermal Non-Equilibrium
PVT	Pressure-Volume-Temperature
REV	Representative Elementary Volume
EOS	Equation of State
VDW	Van der Waals equation of state
RK	Redlich-Kwong equation of state
SRK	Soave-Redlich-Kwong equation of state
PR	Peng-Robinson equation of state
CPA	Cubic Plus Association
SAGD	Steam Assisted Gravity Drainage
HFR	Hot Fractured Rock
TDS	Total dissolved Solids

Thermal and Flow Properties

SYMBOL	DESCRIPTION
T	Temperature (under LTE assumption)
T_f	Fluid Temperature
T_s	Solid (Rock Matrix) Temperature
T_r	Reservoir Initial Temperature
T_{sat}	Saturation temperature at reservoir pressure
T_{C,H_2o}	Critical temperature of water
ρ_m	Bulk Density of porous medium
$(\rho c)_m$	Volumetric heat capacity of the porous medium
$(\rho c)_s$	Volumetric heat capacity of the solid rock
$(\rho c)_f$	Volumetric heat capacity of the fluid
$c_{p,m}$	Specific heat capacity of the porous medium
$\frac{\partial T}{\partial t}$	Rate of change of temperature over time
∇T	Temperature gradient
k_m	Effective thermal conductivity of the medium
k_s	Thermal conductivity of the solid rock
k_f	Thermal conductivity of the fluid
Q	Volumetric heat source or sink term
$q_m^{''}$	Heat flux through the bulk porous medium
$q_s^{''}$	Heat flux through the solid rock
$q_f^{''}$	Heat flux through the fluid
q_j	Volumetric source/sink term for phase j
Pe_d	Péclet number (ratio of advective to diffusive heat transport)

D	Dimensionless dispersion tensor constant
u_m	Mean seepage velocity
$\propto_f$	Thermal diffusivity of the fluid
d_p	Pore diameter
v	Darcy velocity of the fluid
ϕ	Porosity
k	Permeability
μ	Dynamic viscosity of fluid
μ_{water}	Water dynamic viscosity
μ_{inner}	Viscosity of inner zone
μ_{outer}	Viscosity of outer zone
∇P	Pressure Gradient
c_F	Forchheimer form coefficient
$\bar{\mu}\nabla^2 v$	Brinkman viscous term
c_t	Total compressibility
c_w	Water compressibility
c_g	Gas (steam) compressibility
c_f	Formation (rock pore volume) compressibility
n_p	Number of phases
S_j	Saturation of phase *j*
S_W	Water Saturation
U_j	Specific internal energy of phase *j*
u_j	Seepage velocity vector of phase *j*

U_R	Specific internal energy of rock
H_j	Specific enthalpy of phase j
λ_1	Mobility of inner zone
λ_2	Mobility of outer zone
η_{water}	Hydraulic diffusivity of water zone
η_{steam}	Hydraulic diffusivity of steam zone
r_{inv}	Pressure investigation radius during well test

Well Test Parameters

Symbol	DESCRIPTION
R_i	Composite inner radius (radial extent of cold-water bank)
M	Mobility ratio
D	Diffusivity ratio between outer and inner zones
S	Wellbore skin factor
C	Wellbore storage coefficient
kh	Permeability-height product (transmissibility)
P_i	Initial reservoir pressure
ΔP	Pressure difference during well test
ΔP′	Pressure difference derivative during well test

PVT and Equation of State Parameters

SYMBOL	DESCRIPTION
ρ_j	Density of fluid phase j at reservoir conditions
ρ_W	Water density at reservoir conditions
$\rho_{W,ST}$	Water density at stock-tank (surface) conditions

ρ_O	Oil density at reservoir conditions
$\rho_{O,ST}$	Oil density at stock-tank conditions
ρ_g	Gas density at reservoir conditions
$\rho_{G,SC}$	Gas density at standard (surface) conditions
B_W	Water formation volume factor
B_O	Oil formation volume factor
B_g	Gas formation volume factor
R_S	Solution gas–oil ratio (dissolved gas in oil at reservoir conditions)
R_V	Vaporized oil ratio (condensate dissolved in gas at reservoir conditions)
z	Gas compressibility factor (z-factor)
V_m	Molar volume
R	Universal gas constant
P	Pressure
P_{c,H_2O}	Critical pressure of water
$P^v_{H_2O}$	Vapor pressure of water (saturation pressure)
a	Total Helmholtz free energy
a_0	Ideal-gas part of Helmholtz free energy
a_r	Residual part of Helmholtz free energy
α	Dimensionless reduced Helmholtz free energy
α^o	Ideal-gas contribution to reduced Helmholtz free energy
α_r	Residual contribution to reduced Helmholtz free energy
x	Mole fraction of component in mixture
δ	Reduced density
τ	Inverse reduced temperature

$\rho_r(\bar{x})$	Composition-dependent reducing density (GERG-2008)
$\mathrm{T}_r(\bar{x})$	Composition-dependent reducing temperature (GERG-2008)
f_i	Fugacity of component i
Φ_i	Fugacity coefficient of component i
ω	Acentric factor
a_T	Temperature-dependent coefficients in GERG-2008 Helmholtz formulation
b	EOS co-volume parameter
$A_0 - A_7$	Modified PR density correlation coefficients
w_i	Weight fraction of component i
$c_{w,P}$	Pressure-derivative coefficient in water FVF correlation

Chapter 1 – Introduction

1.1. Geothermal Energy and its Global Relevance

Geothermal energy exploits the heat stored in the Earth's interior, topped up continually by radioactive decay and residual planetary heat. Unlike solar or wind, it is not affected by weather cycles: a well-managed geothermal system can deliver baseload electricity around the clock, every day of the year. If the withdrawal and extraction don't go past the natural heat flux, then the "fuel" feels inexhaustible, at least on any timespan that matters for energy planning. Installed geothermal power capacity grew from around 9,791 MWe in 2009 to 16,318 MWe by the end of 2023, and direct-use applications — district heating networks, agricultural greenhouses, decentralized residential heat supply — add further practical value beyond power generation alone (Nkinyam et al., 2025).

1.2. Engineering Motivation: The Cold Front Breakthrough Problem

In geothermal doublet operation, heat extraction involves pumping hot fluid from the reservoir and re-injecting it back into the formation once the thermal energy has been extracted at surface. Reinjection has become a standard and essential practice to safely return produced fluid to the formation, maintain reservoir pressure, and enhance the overall heat recovery factor of the resource (Nkinyam et al., 2025). However, continuous cold-water injection introduces one of the most critical operational risks in geothermal reservoir management: the propagation of a cold waterfront from the injection well towards the production well.

If the doublet is not properly designed or monitored, a premature breakthrough of the cold front can occur. When the cold front reaches the producer, it causes the temperature of the produced fluid to drop and may decrease its enthalpy, and therefore reduce the energy extracted from the geothermal doublet. Therefore, continuously tracking the position and advance rate of the thermal front through the injection well is a primary operational monitoring requirement for sustainable doublet management (Stopa and Wojnarowski, 2006).

1.3. Research Objectives

Building on the monitoring and simulation challenges identified in §1.2, this thesis pursues three specific objectives:

1. Compare the thermal front extension predicted by black-oil based thermal model against the compositional one, quantifying the differences in temperature, viscosity, density, and formation volume factor (FVF) distributions along the sampled inter-well path that are attributable to the model formulation.
2. Conduct a comparison of the equation-of-state formulations and viscosity models available within tNavigator®'s Compositional Thermal model — benchmarking each against the NIST IAPWS-97 thermodynamic reference standard — to identify the most accurate representation of geothermal water properties across the relevant temperature and pressure range and adopt the selected formulation for both compositional and black-oil approach.
3. Simulate a drawdown/build-up test on the injector well — a 12-hour production / 12-hour shut-in sequence — and interpret the resulting pressure transients using a radial composite model in Kappa Ecrin to assess the feasibility of well test for thermal front monitoring in the considered scenarios. The temperature map given by the numerical simulation provides the ground truth against which the well test interpretation accuracy is evaluated.

1.4. Thesis Structure

The remainder of this thesis is organized as follows. Chapter 2 presents the state of the art, reviewing relevant literature on thermal front monitoring in geothermal doublets, the necessity of rigorous thermal modelling, and well test interpretation in thermally heterogeneous systems, and identifies the scope that this thesis addresses. Chapter 3 describes the governing equations for coupled fluid flow and heat transfer, covering both the Temperature model and Compositional Thermal model formulations. Chapter 4 describes the practical setup showing how tNavigator® simulator works, the two modelling approaches, and the calculations of density and viscosity of fluid. Chapter 5 defines the case study geometry and scenarios with the simplified doublet model and operational strategy. Chapter 6 brings everything together and discusses the results.

Chapter 2 – State of the Art

2.1. State of the Art in Thermal Front Monitoring

To manage a geothermal doublet effectively, reliable estimation of the thermal front extension and how fast it is propagating toward the producing well is required. The challenge behind doing so is that the cold front flows in a porous rock matrix at depths of several hundred to several thousand meters through heterogeneous pathways, partially fractured with complex geometrical structure. Four decades of field experience have made one thing clear: no monitoring method works well enough on its own, and each time one approach has shown its limits, operators have had to look for something better.

The most fundamental and historically earliest form of thermal front monitoring is the direct measurement of produced fluid temperature at the production well. A sustained drop in outlet temperature — typically defined as a detectable decrease of 0.2–0.5°C relative to the undisturbed reservoir temperature — constitutes the first observable signal of thermal breakthrough (Sbai and Larabi, 2023). Thermal breakthrough marks the point at which produced fluid temperature begins to decline, progressively reducing heat extraction from the doublet. Modelling studies of the Paris Basin Dogger aquifer have shown that the doublet lifetime is about twice the thermal breakthrough time (Sbai and Larabi, 2023), indicating the importance of detecting breakthrough before it happens rather than after. The limitation of the monitoring production temperature is that by the time the anomaly is detected at the producer, the cold front has already arrived and operational corrective actions like reduction of the injection rate, drilling a new well or removal of the doublet can only be implemented in reaction to an event that has already started. Proactive monitoring, by contrast, aims to estimate the cold front position while it is still safely remote from the producer.

The most widely deployed proactive monitoring technique in geothermal operations is the injection of conservative tracers at the cold-water injector and monitoring of their breakthrough at the production well (Axelsson, 2013). Chemical tracers (fluorescent dyes, halides, alcohols) or stable isotope tracers travel with the injected fluid and provide direct information on inter-well connectivity, dominant flow pathways, and fluid residence time (Axelsson, 2013). From the fluid travel time and an estimate of the thermal retardation factor — which accounts for heat exchange between the injected fluid and the rock matrix and causes the thermal

front to advance more slowly than the fluid front — an approximate thermal breakthrough time can be calculated (Bödvarsson and Tsang, 1982). Reactive tracer methods, in which a temperature-sensitive chemical is used whose degradation rate depends on the local reservoir temperature, offer additional potential for directly tracking the thermal evolution of the inter-well zone rather than just the fluid velocity; however, the effective field application of such methods has not yet been fully demonstrated. Conventional conservative tracer tests therefore provide inter-well connectivity and a thermal breakthrough estimate, but they do not give a direct spatial measurement of the cold front position at the time of the test (USDOE Office of Energy Efficiency and Renewable Energy (EERE) et al., 2011).

In recent years, some of the most advanced pilot projects in geothermal monitoring have made use of distributed temperature sensing (DTS) and distributed acoustic sensing (DAS) systems, deployed via fiber optic cables running along the full length of the wellbore to localize inflow zones and track thermal fronts in real time. DTS provides a continuous temperature profile along the wellbore with spatial resolution of the order of one meter, enabling the detection of cold-water entries from the formation into the injection well and the spatial extent of the thermal anomaly in the near-well region (Schölderle et al., 2021). DAS extends this capability to acoustic and seismic signals, allowing simultaneous detection of inflow zones and hydraulic events. While these technologies are technically impressive, installing and maintaining permanent fiber optic systems in deep, highly deviated, high-enthalpy geothermal wells is an enormously challenging and capital-intensive undertaking, and one that is not feasible for most geothermal operators worldwide. Furthermore, DTS and DAS provide a near-wellbore picture of the thermal state rather than a direct estimate of how far the cold front has advanced into the formation between the injector and the producer (Fokker et al., 2021).

Pressure transient analysis (PTA) — well testing — offers a fourth and arguably underutilized approach to thermal front monitoring. When cold water is injected into a geothermal reservoir, it establishes a region of distinctly different fluid properties around the wellbore: the inner zone (cold, dense, high-viscosity water) is surrounded by the undisturbed hot outer reservoir (low-viscosity water or steam), creating a mobility contrast that imprints a characteristic signature on the pressure transient recorded at the injector during a controlled flow reversal and shut-in sequence. (Stopa and Wojnarowski, 2006) demonstrated analytically that the position of the cold-waterfront in a geothermal reservoir can be related to the composite radius extracted from the log-log pressure derivative diagnostic, using a radial composite reservoir model in which the inner zone and outer zone are characterized by distinct mobilities and storability ratios. This approach was extended to vapor-dominated two-phase reservoirs by (Garg and Pritchett, 1990), who showed that the condensation

front in a steam reservoir undergoing cold-water injection produces a distinct radial composite signature. More recently, harmonic pulse testing (HPT) has been proposed as a variant of this methodology, in which analytical solutions for a moving thermal front are applied to the interpretation of oscillatory pressure signals in aquifer thermal energy storage doublets, allowing the thermal front position and average inter-well temperature to be characterized directly from the pressure response. A significant practical advantage of the PTA approach over all the methods described above is its simplicity of deployment: monitoring via pressure transient analysis requires only standard pressure gauges at the wellhead or downhole, with no permanent optic fibers, no chemical injection, and no laboratory analysis (Fokker et al., 2021).

A proper well test design is essential to guarantee data interpretability. For a geothermal doublet scenario, numerical simulation is needed for synthetic pressure data generation. In commercial geothermal reservoir simulators, at least two distinct thermal model formulations are available — a temperature-dependent black-oil framework and a fully compositional equation-of-state framework — and these may produce different thermal front geometries for the same reservoir scenario. This investigation is the central motivation for the present work.

2.2. The Necessity of Rigorous Thermal Modelling

To accurately interpret pressure transient data and reproduce the radial composite signature of the inner zone, the numerical simulator must correctly resolve the physics of the advancing thermal front. In porous media, the transport of the cold front is governed primarily by advection, with the thermal front advancing more slowly than the fluid front by a thermal retardation factor that reflects the partitioning of heat between the injected fluid and the rock matrix (Stopa and Wojnarowski, 2006). Also, when the cold water contacts the hot rock, altering the temperature and the pore fluid density in the cold-injected zone, the simulator must dynamically update the fluid mobility and storativity to capture the resulting pressure variations. The density difference between the injected cold water and the displaced reservoir fluid is expressed through the formation volume factor $Bw = \rho_{SC}/\rho_{res}$, which the simulator uses to convert the surface injection rate into a reservoir volumetric displacement rate. However, any Bw weak estimation (due to an incorrect determination of reservoir-condition fluid density) will produce a biased estimate of the swept pore volume, and consequently of the simulated cold-front position. It is therefore necessary to accurately represent the temperature-dependent fluid properties to simulate the cold-front accurately.

Historically, there have been a multitude of ways by which geothermal simulators have handled thermal behavior. The main difference is in the computation of fluid properties. Generally, two fluid-description frameworks have been used in reservoir simulation, they are: black-oil model and the compositional model. A thermal formulation can be added to each of these models in order to accommodate temperature as an explicit primary variable, which enables the simulation of in-situ heat transfer, steam generation, and temperature-dependent fluid behavior. There are also differences in the thermal formulation itself. Some formulations anchor fluid properties, most commonly density, to empirical tables at a fixed reference condition. On the other hand, some formulations compute all the thermodynamic quantities dynamically at every grid cell, and for each time step, via equation of state. That choice between simplified and fully EOS-based approaches directly influences how the simulator predicts cold-front geometry in a doublet (Liu et al., 2020).

The accuracy with which a simulator computes water and steam thermodynamic properties, depends critically on the reference formulation it employs. TOUGH2 V2, one of the most widely used geothermal reservoir simulators, originally used the older IFC-67 correlations for vapor pressure, density, and internal energy of liquid water and steam. These correlations came with limitations mostly around 350°C. The more accurate and computationally faster IAPWS-IF97 formulation was subsequently implemented, and the IAPWS-2008 formulation for dynamic viscosity of water and steam was further incorporated, resulting in consistent improvement of accuracy at high temperatures. The IAPWS-IF97 standard, maintained by the International Association for the Properties of Water and Steam, is now recognized as the primary thermodynamic reference for geothermal reservoir simulation, providing water and steam properties with uncertainties of less than 0.02% in density across the temperature range relevant to most geothermal doublet applications (Wagner et al., 2000). The adoption of IAPWS-97 as the thermodynamic formulation in geothermal simulators, together with its use of density and temperature as primary thermodynamic variables, has been shown to give results in agreement with independent simulators, providing confidence for modelling deep geothermal reservoirs (Croucher and O'Sullivan, 2008).

Because water density in simple models is anchored to a fixed reference state rather than being computed dynamically as a function of temperature, simulated volumetric displacement per unit mass of injected fluid is biased in points where local temperature varies and is not equal to the same value at the reference condition. The cold water displacing hot reservoir fluid is denser according to the difference between the temperature of the two fluids, and this difference has a direct

consequence on the way the simulator accounts for injected volumes. The formation volume factor Bw converts surface injection rates into reservoir volumetric rates. This means that fixing the formation volume factor Bw at the undisturbed reservoir temperature rather than evaluating it at the much colder injection temperature, leads to an overestimation of the reservoir volumetric rates injected assigned to each surface cubic meter. Thus, the cold-water bank would therefore appear to be sweeping a larger pore space than it actually does, which means the front position is predicted to be further away from the injector than reality. This is not a theoretical concern: published comparisons of doublet injection simulations run with different thermodynamic formulations show that both the temperature field and the cold-front location shift noticeably depending on which equation of state is used, with codes built on more recent steam table standards consistently predicting different temperature distributions from those relying on older correlations. For vapor-dominated high-enthalpy reservoirs, the situation is further complicated by the phase transition from steam to liquid water at the advancing cold front, which releases latent heat and affects the front velocity in ways that only a fully coupled two-phase EOS-based formulation can correctly represent (Bödvarsson and Tsang, 1982).

Even within EOS-based formulations, additional variability is introduced by the choice of the specific equation of state. Commercial simulators typically have several EOS options available, including Redlich-Kwong (RK), Soave-Redlich-Kwong (SRK), and the GERG-2008 multicomponent formulation. The liquid water density is different for different equations, especially in low temperatures such as in cold-water injection. The cubic equations particularly struggle in the range relative to the IAPWS-IF97 reference (Kunz and Wagner, 2012).

2.3. Reference System: The Larderello-Travale Field

The Larderello-Travale geothermal system in the Colline Metallifere district of southern Tuscany, Italy, holds a unique position in the history of geothermal energy. It is the oldest industrially exploited geothermal field in the world, with commercial electricity generation dating to 1904 and uninterrupted production spanning more than a century (Bertani, 2016). Today the field supplies approximately 30% of the Tuscany region's electricity demand from an installed capacity exceeding 700 MWe (Bertani, 2016), and current production levels are estimated to be sustainable well into the next century (Ebigbo et al., 2016; Romagnoli et al., 2010).

The reservoir is vapor-dominated, extending to depths of 1,000 to 4,000 m, with temperatures above 200°C and pressures of 10–30 bara (Della Vedova et al., 2008; Romagnoli et al., 2010). It is dominated by dry or superheated steam, with liquid water

only showing up in scattered pockets or as condensate. This makes Larderello-Travale, a natural reference point for understanding how high-enthalpy vapor-dominated systems behave. However, many across Europe, including the Dogger aquifer doublets in the Paris Basin and the sedimentary systems of the Po Plain and Bavaria, operate under different conditions with higher pressures (50–150 bar), lower temperatures (60–150°C) and fully liquid water filling the reservoir. These systems are being developed more for district heating and binary power generation (Lund and Toth, 2021). This contrast between two thermodynamic extremes is precisely what motivates the two-case structure of this study: a low-enthalpy liquid-dominated scenario representative of deep aquifer systems, and a high-enthalpy vapor-dominated scenario inspired by Larderello-Travale, examined side by side.

2.4. Well Testing and Radial Composite Interpretation in Geothermal Systems

Pressure transient analysis provides reservoir characterization without additional drilling by recording the pressure response at a well during and after a controlled change in flow rate and analyzing the resulting signal on a logarithmic time scale. One of the most important developments in well test interpretation was the introduction of the pressure derivative by Bourdet et al. (1989). This is simply the logarithmic time derivative of the pressure change but plotting it alongside the pressure difference on a log-log scale turned out to be remarkably powerful. Features that would be completely invisible on a standard semi-log plot become readable on the log-log derivative, giving the engineer a much more direct way to identify what flow regime the reservoir is in at any given moment. In a clean, homogeneous reservoir, radial flow produces a flat derivative plateau whose level is proportional to the formation transmissibility while deviations from this plateau, upward trends, downward trends, or transitions between two stabilization levels, indicate boundaries, heterogeneities, or changes in fluid properties away from the well.

When a well is surrounded by a zone of altered fluid or rock properties, the pressure transient successively samples the inner zone and then the outer region, producing two stabilization levels on the log-log derivative plot separated by a transition region. This composite reservoir geometry was first described analytically in the petroleum engineering literature by Hurst (1953) in the context of fluid banks formed during waterflood injection and was formalized as the radial composite model by subsequent authors including Satman et al. (1980), who derived Laplace-space analytical solutions for a well centered in a circular inner zone of mobility M surrounded by an infinite outer reservoir of differing mobility

and diffusivity. The composite radius Ri represents the radial distance of the inner zone and plays an important role in the pressure-transient response. The shift between the two derivative plateau levels starts when the pressure disturbance reaches Ri. The time at which this transition occurs depends on the term $\frac{\phi\mu ctRi^2}{k}$ (Satman et al., 1980).In addition, the ratio between the two stabilized derivative levels gives the mobility ratio, (M), between the outer and inner zones. This ratio helps indicate the difference in transmissibility across the composite boundary.

The reason for using the radial composite model in geothermal injection wells is clear. When cold water is injected continuously, it gradually forms a colder and more viscous water zone around the injection well. This zone is then surrounded by the original warmer reservoir, which has lower viscosity and higher mobility. Stopa and Wojnarowski (2006) showed analytically that this thermal contrast creates a radial composite pressure response. In this case, the composite radius, (R_i), represents the location of the cold-water thermal front. By identifying this radius from the log-log pressure derivative plot, it is possible to estimate the movement of the cold front in a non-invasive way. Garg and Pritchett (1990) applied a similar idea to vapor-dominated two-phase geothermal reservoirs. They showed that the condensation front between steam and water can also create a composite pressure response. Because cold liquid water is much more viscous than superheated steam, the mobility contrast is very large, causing a strong drop in the pressure derivative at the composite transition. Together, these studies show that well testing can be a useful operational method for monitoring cold-front movement, alongside tracer tests and distributed sensing methods discussed in §2.1.

A radial composite well test on an injection well can provide four main parameters. These are the formation permeability k, which is obtained from the inner-zone derivative plateau; the composite radius Ri, which is identified from the time when the derivative starts to transition; the mobility ratio, (M), which is calculated from the difference between the outer- and inner-zone derivative levels and the wellbore skin factor S which is estimated from the early-time deviation from the unit-slope wellbore storage line. Among these parameters Ri is the most important for managing a geothermal doublet because it indicates the position of the cold front at the time of the test. By dividing Ri by the total injection time, the average speed of cold-front movement can be estimated. Then by dividing the distance between the injector and producer by this speed, the expected time of thermal breakthrough can be predicted.

Although the radial composite model is useful, it has major drawbacks when it is used with thermally dynamic geothermal systems. The analytical solution assumes a sharp, static step-change in fluid properties at Ri: the transition from cold

inner zone to warm outer zone occurs instantaneously at a fixed radius, whereas the actual viscosity profile in the reservoir varies continuously with temperature across a transition zone spanning tens of meters. This gradual transition means that the pressure transient integrates the mobility gradient rather than detecting a single discrete boundary, which can cause the composite radius extracted from Kappa to differ from the temperature isotherm that defines the cold zone in the simulator (Stopa and Wojnarowski, 2006). Additionally, during shut-in, cold water starts to heat up, which changes the viscosity of the inner zone. This goes against the static property assumption of the composite model which makes the late-time pressure derivative deviate from the analytical prediction. However, these limitations do not mean that the approach is invalid, but that the match window needs to be carefully selected, and then the extracted Ri has to be interpreted as an effective composite radius instead of a precise thermal front position.

Chapter 3 – Governing Equations

To simulate how heat and fluid move together through a geothermal reservoir, three coupled sets of equations must be solved simultaneously: mass conservation, momentum conservation, and energy conservation (Khait and Voskov, 2018).

Heat transfer in porous media occurs via conduction through the solid and fluid phases, and convection carried by the moving fluid. The simulation of thermal processes in porous media can be categorized by how the temperature field is treated regarding the solid and fluid phases. The standard energy equation assumes Local Thermal Equilibrium (LTE) — that is, the solid temperature and the fluid temperature ((i.e., T_s and T_f respectively) are identical at any point in the domain, so a single temperature field T describes both phases. This holds well at reservoir scale, where heat transfer between the solid matrix and the saturating fluid is sufficiently rapid that any temperature difference between them equilibrates instantly. Where fluid velocities are very high or thermal transients are rapid, however, this equilibration is no longer guaranteed, and a Local Thermal Non-Equilibrium (LTNE) model becomes necessary: the solid and fluid temperatures are tracked separately by two coupled energy equations, linked by an interphase heat transfer coefficient that quantifies how quickly heat passes between them (Bejan, Adrian, 2006).

The two main frameworks used to handle fluid behavior and thermal transport in reservoir simulation are: the Temperature model and the Compositional Thermal model. The Temperature model takes the reservoir fluid as up to three bulk phases: gas, oil, and water. Then the thermodynamic quantities (density and formation volume factors) are read from predefined PVT tables taken at reference conditions. This allows it to be faster and more computationally robust; however, the fluid description is not as detailed. It fixes the composition of each phase and doesn't compute compositional changes due to temperature and pressure.

The Compositional Thermal model, on the other hand, does not operate with bulk phases, but rather tracks the molar concentration of each chemical component. Then it uses the equation of state with the composition to compute phase equilibrium at each grid cell and timestep. This allows the model to determine, from first principles, how the mixture partitions between liquid and vapor, as conditions change, even during phase transitions, where the simpler bulk-phase description of the Temperature model breaks down.

The following sections define and compare these governing equations for each model.

3.1. Thermal Equations

Both the Temperature and Compositional Thermal model formulations solve a form of energy conservation equation for the fluid-saturated porous medium, but they differ fundamentally in the choice of primary thermodynamic variable, a distinction whose physical consequences are detailed in the following subsections.

3.1.1. Temperature (Black Oil) Model – Energy Formulation

The fundamental law governing conduction is **Fourier's law**, which states that the rate of heat conduction is proportional to temperature gradient (Çengel, 2003). In porous medium, however, conduction follows a tortuous path through the solid matrix and the fluid-filled pores. Therefore, an effective thermal conductivity (k_m) is required to describe the medium as a continuum (Bejan, Adrian, 2006):

$$\rho_m c_{p,m} \frac{\partial T}{\partial t} = \nabla \cdot (k_m \nabla T) + Q \quad (1)$$

Where ρ_m= matrix density, $c_{p,m}$ = matrix heat capacity.

The energy conservation equation for a fluid-saturated porous medium follows from the first law of thermodynamics applied to a Representative Elementary Volume (REV), the smallest volume over which meaningful continuum properties can be defined in a porous medium. The resulting heat flux has two contributions: a conductive term governed by Fourier's law (Eq. 1), and a convective term carried by the moving fluid. Substituting these conductive and convective flux contributions into the energy balance, and applying the LTE assumption, gives the governing equation for the porous medium:

$$\frac{(\rho c)_m \partial T}{\partial t} + (\rho c_p)_f v \cdot \nabla T = \nabla \cdot (k_m \nabla T) + q_m'' \quad (2)$$

Where $(\rho c)_m$ represents the average heat capacity of the porous medium weighted by the porosity (ϕ) and the fraction of the matrix occupied by different solid components:

$$(\rho c)_m = (1-\phi)(\rho c)_s + \phi(\rho c_P)_f \quad (3)$$

Where *s* and *f* refer to the solid and fluid phases, respectively. While $(\rho c_P)_f$ represents the heat capacity of the fluid at constant P.(Bejan, Adrian, 2006).

Moreover, v is the Darcy (seepage) velocity vector, which arises from volume averaging over a (REV), large enough to smooth out pore-scale heterogeneities yet small enough to capture macroscopic gradients. Unlike the intrinsic pore velocity, which represents the average fluid speed within the pore space alone, the Darcy velocity represents the volumetric fluid flux per unit total cross-sectional area of the bulk medium — solid and fluid combined. Both are related through porosity by:

$$v = \frac{Q}{A_{total}} = \phi v_{pore} \quad (4)$$

And k_m symbolizes the overall (effective) thermal conductivity of the porous medium. This stands for the aggregate ability of the fluid-saturated matrix to conduct heat. For simple parallel conduction, it is defined as the weighted arithmetic mean:

$$k_m = (1-\phi)k_s + \phi k_f \quad (5)$$

q''_m stands for the overall heat production per unit volume of the medium. Like heat capacity, this is a volume-averaged source term between the internal heat generation rates (e.g., from chemical reactions or nuclear decay) of solid and fluid phases defined as:

$$q"_m = (1-\phi)q"_s + \phi q"_f \quad (6)$$

In regimes with high fluid velocity, the hydrodynamic mixing of the interstitial fluid enhances heat transfer. This phenomenon, known as thermal dispersion, is often modelled by augmenting the molecular thermal diffusivity with a dispersive term that depends on the **Péclet** number Pe_d and the particle diameter. Consequently, the effective thermal conductivity k_m in (Eq. 1) is replaced by a total effective conductivity tensor k_{eff} to account for the mechanically enhanced heat transfer (Bejan, Adrian, 2006).

$$k_{eff} = k_m + Dk_f Pe_d \quad (7)$$

Where D is a dimensionless dispersion tensor constant and Pe_d is the Péclet number based on the particle/pore diameter, defined as $Pe_d = \frac{u_m d_p}{\propto_f}$, where u_m is the mean seepage velocity, d_p is the particle/pore diameter, and $\propto_f$ is the thermal diffusivity of the fluid.

For the simulated conditions, Darcy velocities of order 10^{-6} m/s (Case 1) to 10^{-8} m/s (Case 2) at a representative radial distance of 50 m, and a grain size of order 10^{-3} m, the pore-scale thermal Péclet number $Pe_T = \frac{\mathrm{v\,d}}{\alpha_f}$ remains small of order 10^{-2} or below verifying that mechanical thermal dispersion is neglected with respect to molecular conduction and not applying the dispersive correction in (Eq. 7). Effective conductivity is therefore well approximated by the molecular value (Eq. 5). In the Temperature (TEMP) model, temperature T serves directly as the primary energy variable, which is sufficient for single-phase or non-boiling systems where T uniquely characterizes the thermodynamic state of the fluid.

3.1.2. Compositional Thermal model

Equation 2 is adequate when temperature alone defines the fluid's local thermodynamic state, i.e., under single-phase conditions where a given T and P correspond to a unique set of fluid properties. In systems where liquid water boils into steam, however, temperature is no longer a sufficient primary variable: at constant pressure, the saturation temperature T_{sat} is fixed regardless of the vapor quality which ranges from 0 (saturated liquid) to 1 (saturated vapor). These two endpoints are thermodynamically distinct; their specific enthalpies differ by approximately 2,257 kJ/kg yet are indistinguishable by temperature alone. A primary variable that varies continuously through a phase change and uniquely characterizes the thermodynamic state is therefore required to close the energy equation in two-phase systems. The Compositional Thermal model on the other hand, resolves this by adopting internal energy and enthalpy as primary thermodynamic variables (Zaydullin, 2014). The energy conservation equation therefore takes the following general form, coupling fluid enthalpy transport with rock internal energy storage:

$$\frac{\partial}{\partial t}\left(\emptyset \sum_{j=1}^{n_p} U_j \rho_j S_j + (1-\emptyset) U_R \right) - \nabla \cdot \left(\sum_{j=1}^{n_p} H_j \rho_j u_j \right) - \nabla \cdot (\kappa \nabla T) + \sum_{j=1}^{n_p} H_j \rho_j q_j = 0 \qquad (8)$$

Where U_R represents the internal energy of the rock (solid matrix), κ corresponds to the effective thermal conductivity of the porous system (rock-fluid system), and n_p is the number of phases present in the system (e.g., water, oil, gas). For each fluid phase j, the variables $U_j, \rho_j, S_j, H_j, and\ u_j$ denote the internal energy, density, saturation, enthalpy, and seepage velocity vector, respectively. Lastly, q_j refers to the source/sink term being the injection or production rate of phase j per unit volume (e.g., well terms).

Concerning the physical meaning of the governing equation, the terms can be divided into four fundamental mechanisms of energy transfer and storage:

- **The Transient Term** $\left[\frac{\partial}{\partial t}\left(\phi \sum_{j=1}^{n_p} U_j \rho_j S_j + (1-\phi) U_R\right)\right]$ represents the rate of accumulation of total internal energy within the control volume, accounting for both the saturating fluid mixtures and the solid rock matrix.
- **The Convective Transport Term** $\left[\nabla \cdot \left(\sum_{j=1}^{n_p} H_j \rho_j u_j \right)\right]$ describes enthalpy carried into or out of the control volume by the moving fluid phase which is

considered as the dominant mode of energy transport in a flowing geothermal reservoir.

- **The Conductive Term** $[\nabla \cdot (\kappa \nabla T)]$ reflects the heat transfer caused by temperature gradients through the bulk volume of the rock using Fourier's law (Bejan, Adrian, 2006).

  The Source/Sink Term $\left[\sum_{j=1}^{n_p} H_j \rho_j q_j\right]$ addresses the added or removed energy due to the presence of external operations, mainly the enthalpy of fluids injected or produced at the wells.

3.2. Mass Conservation

The governing equations of reservoir simulation are based on the conservation of mass for each fluid phase. For a multiphase porous medium system, the continuity equation for phase j states that the rate of mass accumulation within a control volume equals the net mass flux across its boundaries plus any source or sink contributions from wells:

$$\frac{\partial(\phi \rho_j S_j)}{\partial t} + \nabla \cdot (\rho_j u_j) = \rho_j q_j \qquad (9)$$

where ϕ is the porosity of the rock, ρ_j is the density of phase j at reservoir conditions, S_j is the saturation of phase j (the fraction of pore volume occupied by that phase), u_j is the seepage velocity vector of phase j, and q_j is the volumetric source or sink term per unit bulk volume representing well injection or production. The saturations of all phases must satisfy the constraint:

$$\sum_{j=1}^{n_p} S_j = 1 \qquad (10)$$

where n_p is the total number of fluid phases present (water, oil, gas).

The transient term $\frac{\partial}{\partial t}(\phi \rho_j S_j)$ captures both compressibility effects — as pressure changes alter ρ_j and ϕ — and displacement effects, as saturation S_j changes due to multiphase flow. In the geothermal context of this work, thermal expansion and contraction directly modify ρ_j through the thermodynamic model, creating a coupling between the mass conservation and energy conservation equations that is the fundamental source of the differences between the Temperature and Compositional Thermal model formulations examined in this thesis. Specifically, in the Temperature (TEMP) model, ρ_j is governed solely by the

pressure-dependent PVTW formation volume factor and does not respond to temperature changes; in the Compositional Thermal model (THERMAL), ρ_j is computed dynamically from the GERG-2008 equation of state, making the mass balance inherently temperature sensitive.

3.3. Flow Equations

The motion of fluid through the porous matrix is governed by the conservation of momentum. The most fundamental constitutive equation for this flow is **Darcy's Law**, which relates the seepage velocity vector (v) to the pressure gradient (∇P) and the gravitational body force (ρg):

$$v = -\frac{k}{\mu}(\nabla P - \rho g) \quad (11)$$

Where k is the permeability of the medium and μ is the dynamic viscosity of the fluid (Bejan, Adrian, 2006). Darcy's law is valid for low velocity flows where Reynolds numbers are small (typically Re<1).

At higher flow velocities, inertial forces become significant and the linear pressure–velocity relationship of Darcy's law no longer holds. The Forchheimer equation captures this by adding a quadratic drag term to the momentum balance, making it appropriate for near-wellbore regions where velocities are elevated, tight or low-permeability formations, naturally fractured systems, high-rate injection operations such as enhanced oil recovery, hydraulic fracturing, or CO_2 sequestration, and situations where formation damage from fines migration or scaling has further restricted flow paths. In these cases, the Forchheimer equation provides a more accurate description of fluid dynamics than Darcy's law:

$$\nabla P = -\frac{\mu}{k}v - c_F k^{-\frac{1}{2}}\rho|v|v \quad (12)$$

Where c_F is a form coefficient related to the geometry of the porous medium (Bejan, Adrian, 2006).

Where viscous shear stresses at the pore walls become significant, the Brinkman equation extends Darcy's law by adding a **Laplacian** viscous term ($\bar{\mu}\nabla^2 v$) to the momentum balance. This allows the no-slip condition to be enforced

at solid interfaces — something the standard Darcy formulation cannot do — and makes the model applicable across both the porous matrix and macroscopic open regions such as fractures and karst cavities. For this reason it is sometimes called the **Stokes-Brinkman** or **Darcy-Stokes-Brinkman** equation, reflecting its role as a bridge between porous-medium flow and free-fluid flow (Bejan, Adrian, 2006). It is especially useful in highly heterogeneous reservoirs, where free flow in fractures interact with Darcy flow in the surrounding matrix, allowing a seamless transition between flow regions without explicit interface modeling. In this work, however, the Brinkman formulation is not applied, as fluid flow in the geothermal reservoir studied here operates well within the Darcy flow regime, where viscous forces dominate and wall shear effects at solid interfaces are negligible (HE, 2017).

$$\nabla P = -\frac{\mu}{k} v - c_F k^{-\frac{1}{2}} \rho |v| v - \bar{\mu} \nabla^2 v \qquad (13)$$

For the fluid flow in the high-enthalpy geothermal doublet reservoir that will be studied later, it will be modelled using Darcy's law, originally formulated by Henry Darcy. This assumption is justified because, despite the high thermal energy of the system, fluid motion in porous geothermal formations typically occurs at low pore-scale Reynolds numbers, where viscous forces dominate over inertial effects. At the reservoir scale, the continuum approximation applies and momentum transfer can be accurately described by the linear pressure-velocity relationship of Darcy flow. Non-Darcy effects, such as those described by the Forchheimer correction (Bejan, Adrian, 2006), are generally confined to near-wellbore regions or highly fractured zones and are not expected to significantly influence the large-scale thermohydraulic behavior that is the focus of this work. Adopting Darcy's law (Eq. 11) therefore ensures physical consistency while maintaining computational efficiency and model robustness for the analysis of heat extraction and long-term reservoir performance.

3.4. Thermodynamic Properties

The equation of state provides the relationship between thermodynamic variables (such as Pressure, Volume, and Temperature), thus allowing the characterization of density variations as a function of temperature and pressure.

3.4.1. Black-oil Temperature model

The Black-oil Temperature model is a simplified empirical formulation widely used in petroleum reservoir simulation. Unlike Compositional Thermal models (which are discussed later) that rely on fundamental thermodynamic equations of state, the black-oil approach utilizes pressure-dependent PVT relationships (acquired from laboratory measurements) to describe phase behavior. It expresses fluid properties via formation volume factors and solution gas ratios, and computes densities from standard-conditioned values corrected by these empirical factors. The black-oil model is quite reliable and is computationally fast when used for conventional isothermal oil and gas applications. However, it is not designed to accommodate thermal changes, so it produces inaccuracies for systems where temperature changes affect critical parameters, for example, when heat transfer induces phase changes, or when the fluid composition shifts significantly with temperature. In these situations, it is no longer valid to use solely pressure-dependent PVT tables, as such a model would incorrectly describe the reservoir behavior. The same applies for high-enthalpy geothermal systems, which is why the Temperature model requires careful validation in order to be ensure accuracy, and it's understood that it can be completely invalid in some conditions.

Fluid densities in the black-oil framework are defined as follows:

- Oil:

$$\rho_0 = \frac{\rho_{O,ST} + R_s \rho_{G,SC}}{B_o} \quad (14)$$

Where ρ_0 = Oil density in reservoir conditions, $\rho_{O,ST}$ = Oil density in Stock Tank conditions, R_s = Fraction of Gas dissolved in Oil, $\rho_{G,SC}$ = Gas density in Standard Conditions, B_o= Oil formation volume factor.

R_s and B_o are calculated using Oil **Standing's** correlations in case of 2-phase model (Dead Oil), and experimental in the other case (i.e., Live Oil (3-phase)) (Bahadori, 2017).

- Gas:

$$\rho_g = \frac{\rho_{g,SC} + R_v \rho_{O,ST}}{B_g} \quad (15)$$

Where ρ_g = Gas density in reservoir conditions and B_g= Gas formation volume factor, R_v = Fraction of Oil vaporized in Wet Gas.

$$B_g = 0.02827 \frac{zT}{14.5037P} \quad (16)$$

Where z = Gas compressibility factor calculated by **Standing** or **Hall – Yarborough's correlations** (Kareem, 2014), T = Reservoir Temperature in ^{o}R, and P = Reservoir initial Pressure in bara.

- Water:

$$\rho_w = \frac{\rho_{w,ST}}{B_w} \quad (17)$$

Where ρ_w = Water density in reservoir conditions, $\rho_{w,ST}$ = Water density in stock tank conditions, and B_w = Water formation volume factor at the reference pressure and compressibility that is defined by:

$$c_w = -\frac{1}{B_w}\frac{\partial B_w}{\partial P}. \quad (18)$$

3.4.2. Compositional Thermal model

In compositional reservoir simulation, the thermodynamic state, fluid properties, and instantaneous phase equilibrium of a multicomponent mixture are governed by an **EOS**. Historically, the development of EOS for petroleum engineering applications has been dominated by **cubic equations**, which provide a mathematical relationship between pressure, molar volume, and temperature.

The foundation for modern cubic EOS was set up by **Van Der Waals (VDW) Equation in 1873**, which was the first model capable of representing vapor-liquid coexistence by introducing parameters to account for molecular repulsion and intermolecular attraction. While groundbreaking, the **VDW EOS** was largely qualitative and lacked the precision needed for complex hydrocarbon mixtures. (van der Linden, 2015).

To achieve qualitative accuracy, a series of modifications to the attractive pressure term were developed over the following century, leading to the classical cubic equations of state that are widely implemented in modern reservoir simulations today: (Young, 2022)

- **Redlich-Kwong (RK, 1949):** Redlick and Kwong significantly improved the prediction of gas-phase properties by introducing a temperature-dependent modification to the attractive term of the VDW equation.

- **Soave-Redlich-Kwong (SRK, 1972):** Also known as Redlich-Kwong-Soave (RKS) equation. The main change compared to the original RK equation is that it replaced the original temperature term with a more generalized temperature-dependent function (α) that incorporated the acentric factor (ω). This term, introduced by Pitzer, accounts for the non-spherical shape of molecules. Vapor pressures and phase equilibrium prediction for hydrocarbon mixtures were significantly improved by this change.
- **Peng-Robinson (PR, 1976):** Peng and Robinson proposed a further modification to the attractive term denominator to improve the prediction of liquid densities and fluid behavior near the critical point. Today, the **PR EOS**, alongside **SRK**, is still a standard industry for general compositional reservoir simulations.

$$P = \frac{(R\,T)}{(V_m - b)} - \frac{a(T)}{\left(V_m(V_m + b) + b\,(V_m - b)\right)} \qquad (19)$$

Where $a(T), b$ = EOS parameters, V_m = Molar volume, R = Gas constant, T = System's absolute temperature, P = System's pressure.

While classical cubic equations (**RK**, **SRK**, **PR**) are computationally efficient and robust for standard oil and gas systems, they show limitations when applied to highly polar fluids or associating molecules, such as water, alcohols, and glycols (*tNavigator® Technical Reference Manual*, 2024). Because these substances form complex hydrogen bonds, simulators often apply advanced extensions, such as the **Cubic Plus Association (CPA)** models (e.g., PR-CPA or SRK-CPA). These models augment the traditional cubic EOS with an additional mathematical term specifically designed to describe the chemical equilibria of associative intermolecular bonds. So, if the simulation treats water as a hydrocarbon-like, pure and single component interacting with other gases (such as in a dedicated Gas-Water system) the model may utilize a **modified PR EOS.** Because the standard PR coefficient (α) fails for water, it is substituted with a specialized, temperature-dependent **Polynomial function** combined with an **exponential pressure compressibility term**:

$$\rho_W = \frac{A_0 + A_1 T + A_2 T^2 + A_3 T^3 + A_4 T^4 + A_5 T^5}{1 + A_6 T} * e^{c_{w,P}(P - A_7)} \quad (20)$$

Where T is the temperature, and $A_0, \ldots, A_7$ are predefined empirical constants for water, and $c_{w,P}$ is the water compressibility (*tNavigator® Technical Reference Manual*, 2024).

On the other hand, if the reservoir involves highly saline brine with dissolved non-condensable gases (like CO2), pure water may not be sufficient. When modelling the solubility of multiple components in the aqueous phase, the simulator modifies the pure water density to account for the solutes using **Ezrokhi's Method**:

$$log\ \rho w\ =\ log\ \rho_0\ +\ \Sigma A_i w_i \quad (21)$$

Furthermore, for applications demanding extreme precision in gas-phase properties — such as complex natural gas injection or high-enthalpy geothermal systems — standard cubic equations must be substituted with highly specialized, multi-parameter, non-cubic models. (Young, 2022). Consequently, modern high-performance simulators like tNavigator® support advanced thermodynamic

formulations, including the **GERG-2008,** developed by the European Gas Research Group, to accurately govern complex multicomponent mixtures across wide pressure and temperature ranges (*tNavigator® Technical Reference Manual*, 2024). This approach takes each component individually and computes phase equilibrium through **fugacity** equality, allowing correct modelling of gas-rich geothermal systems or reservoirs containing non-condensable gases. The Compositional Thermal model is therefore more general and physically rigorous, especially for systems with strong compositional effects. Nevertheless, it is computationally more demanding, introduces additional numerical nonlinearity, and requires reliable compositional data, which may not always be available (Farzaneh-Gord et al., 2021).

On the other hand, in such systems (i.e., high-enthalpy geothermal reservoirs), water boils into steam. To model this within a compositional framework, H_2O must be explicitly declared as a chemical component. The phase equilibrium between liquid water and steam is then determined by calculating the fugacity of water, independent of the **GERG-2008 equation** used for other gases (*tNavigator® Technical Reference Manual*, 2024). The equilibrium relies heavily on water saturation pressure $P^v_{H_2O}$ which is calculated dynamically based on the critical temperature T_{c,H_2O} and critical pressure P_{c,H_2O} of water using a high-order polynomial:

$$\ln\left(\frac{P^v_{H_2O}}{P_{c,H_2O}}\right) = \frac{T_{c,H_2O}}{T}(-7.85823\tau + 1.83991\tau^{1.5} - 11.7811\tau^3 + 22.6705\tau^{3.5} - 15.9393\tau^4 + 1.77516\tau^{7.5}) \quad (22)$$

Where $\tau = 1 - \frac{T}{T_{c,H_2O}}$. The fugacity coefficient of water is then derived from this saturation pressure to figure out exactly how much water transitions into steam.

GERG-2008 is explicit in the **Helmholtz free energy (a)**. It defines the free energy as a function of density, temperature, and mixture composition.

$$a(\rho, T, \bar{x}) = a^0(\rho, T, \bar{x}) + a^r(\rho, T, \bar{x}) \quad (23)$$

In computational practice, this equation is evaluated in its dimensionless form ($\alpha = \frac{a}{RT}$), using the reduced fluid density (δ) and the inversed reduced mixture temperature (τ).

(24)

$$\alpha(\delta, \tau, \bar{x}) = \alpha^0(\delta, \tau, \bar{x}) + \alpha^r(\delta, \tau, \bar{x})$$

Where the reduced parameters are defined as:

- $\delta = \frac{\rho}{\rho_r(\bar{x})}$
- $\tau = \frac{\mathrm{T}}{\mathrm{T}_r(\bar{x})}$

Such that $\rho_r(\bar{x})$ and $\tau_r(\bar{x})$ are composition-dependent reducing functions for density and temperature, respectively.

The primary advantage of the Helmholtz free energy formulation is that all necessary macroscopic thermodynamic properties of the mixture can be obtained by combining various derivatives of the reduced **Helmholtz free energy**. For instance, the gas compressibility factor (z-factor) is derived directly from the partial derivative of the residual part with respect to the reduced density.

$$z = \frac{P}{\rho RT} = 1 + \delta\alpha_\delta^r \quad (25)$$

Where α_δ^r is the partial derivative of the residual part of the dimensionless Helmholtz free energy with respect to the reduced density δ: $\alpha_\delta^r = \left(\frac{\partial \alpha^{\mathrm{r}}}{\partial \delta}\right)_{\{\tau,x\}}$, such that α^{r} is the residual (non-ideal) part of the dimensionless Helmholtz free energy and it captures all departures from ideal-gas behavior due to intermolecular interactions.

Similarly, to establish the vapor-liquid equilibrium (the thermodynamic balance between the phases during a flash calculation), the model derives the fugacity (f_i) and the fugacity coefficient ($\emptyset_i$) for each individual component using the derivatives of the residual **Helmholtz free energy** with respect to the number of moles (*tNavigator® Technical Reference Manual*, 2024).

$$\ln \emptyset_i = \left(\frac{\partial(n \cdot \alpha^{\mathrm{r}})}{\partial n_{\mathrm{i}}}\right)_{\{T,V,n_{\mathrm{j}}\neq_{\mathrm{i}}\}} - ln\, z \quad (26)$$

Where $\left(\frac{\partial(n\cdot\alpha^{r})}{\partial n_{i}}\right)_{\{T,V,n_{j\neq i}\}}$ is the partial derivative of the total mixture residual Helmholtz energy ($n\cdot\alpha^{r}$, where n is total moles) with respect to the mole number of component i, at constant temperature, volume, and mole numbers of all other components $j \neq I$ which captures how adding one more mole of component i changes the non-ideal energy of the mixture, and $(-\ln z)$ subtracts the compressibility factor contribution, converting from a volume-based reference to a pressure-based one.

By dynamically solving these derivatives during the simulation, the **GERG-2008** accurately governs the phase behavior and density evolution of the reservoir fluids without relying on standard PVT tables.

3.5. Boundary Conditions

3.5.1. Thermal Boundary Conditions:

To begin with the thermal equations, the standard boundary conditions include (Bejan, Adrian, 2006; Çengel, 2003):

- **Specified Temperature (Dirichlet)**: The surface boundary is maintained at a fixed, prescribed temperature.
- **Specified Heat Flux (Neumann)**: A specified heat flux can also be imposed across the boundary — the most common instance being a thermally insulated surface, where the temperature gradient normal to the boundary is set to zero and no heat crosses it.
- **Interface Conditions**: At the interface between two different media — for example, between a porous region and an adjacent free fluid — the LTE assumption requires that both temperature and the normal component of heat flux remain continuous across the boundary (Bejan, Adrian, 2006).

3.5.2. Hydrodynamic Boundary Conditions:

For the fluid flow (mass and momentum) equations coupled with the thermal model, standard outer reservoir boundaries are governed by:

- **Constant Pressure (Dirichlet)**: The pressure of the phase (P) is maintained at a specific value at the boundary (*tNavigator® Technical Reference Manual*, 2024).

- **No-Flow (Neumann)**: The boundary is treated as impermeable, meaning the pressure gradient normal to the boundary is zero, and consequently, the normal component of the phase velocity vanishes (*tNavigator® Technical Reference Manual*, 2024).

Chapter 4 – Numerical Simulation

Having established the governing equations in Chapter 3, this chapter describes how these formulations are implemented in the tNavigator® simulator.

tNavigator® (*tNavigator® Technical Reference Manual*, 2024) is a commercial full-field reservoir simulator designed for multi-phase, multi-component fluid flow and heat transfer in porous media. The software is developed by Rock Flow Dynamics (RFD) and has a unified computational framework which includes multiple models: black-oil, compositional, and thermal formulations. It is commonly used in the petroleum industry, but also in the geothermal domain, for applications related to reservoir characterization and production forecasting. It's selection for this study is due to its ability to natively implement the Temperature model (TEMP) as well as the Compositional Thermal model (THERMAL), thus a direct comparison of the two models can be performed while maintaining purely identical reservoir geometry, rock properties, and operational conditions. The following sections detail the fluid property models selected for density and viscosity and explain how cumulative volumetric rates are computed in each modeling framework.

4.1. Modelling Approaches

The software tNavigator® offers two different modelling approaches accounting for temperature evolution in space and time T (x, y, z, t): Thermal modelling, based on compositional formulation, which solves the full energy equation accounting for enthalpy transport, and Temperature modelling, based on black-oil formulation, which assumes that temperature variations are transported primarily by advection with the fluid and solves the energy equation with temperature T as the primary variable, capturing both advective and conductive heat transport, but without representing phase transitions or the associated latent heat exchange. LTE is strictly assumed in both cases.

A complete side-by-side reference of the tNavigator® keywords governing each formulation — covering phase handling, PVT inputs, viscosity and density models, thermal conductivity, relative permeability, and energy injection/production tracking — is provided in Appendix A.

4.2. Water Density Modelling in Geothermal Reservoir Simulation

Getting the formation volume factor (Bw) right is one of the most consequential aspects of simulating a geothermal doublet correctly. Bw governs how the simulator converts the surface injection rate into a reservoir volumetric displacement rate; if Bw is biased, the volumetric sweep of the cold-water bank is biased, and the simulated cold-front position will be systematically offset. The underlying physical reason Bw may be wrong is that the PVTW table anchors the reservoir-condition density at the initial reservoir temperature. The mathematical framework used to compute Bw — and therefore the simulated cold-front geometry — differs fundamentally depending on whether a simplified Temperature or a rigorous Compositional Thermal model is employed.

4.2.1. Temperature model

In standard Temperature models, the simulator simplifies the reservoir fluid into bulk macroscopic phases and avoids phase equilibrium calculations. It utilizes predefined empirical PVT tables instead of determining density dynamically via thermodynamic state variables.

Then it computes water mass density at reservoir conditions by dividing a fixed stock-tank density by the pressure-dependent Formation Volume Factor for water (FVFW).

The FVFW is related to the fluid's isothermal compressibility via the derivative. While computationally highly efficient and robust for conventional, isothermal liquid systems, this framework has a significant limitation in high-enthalpy geothermal applications: the FVFW tables are strictly governed by pressure. Consequently, the Temperature model fundamentally ignores the dramatic density changes and volumetric expansion that occur during temperature shifts and phase changes (e.g., steam condensing into liquid water), making it unsuitable for multi-phase systems.

4.2.2. Compositional Thermal model

To capture the complex phase changes driven by heat transfer, advanced geothermal models utilise a Compositional framework. This approach abandons static PVT tables, tracking the actual molar concentration of individual chemical components and computing phase equilibria dynamically using an EOS.

To select the most appropriate density formulation for water in the Compositional Thermal model, Figure 1 compares the density predictions of the equations of state available in tNavigator® — Redlich–Kwong (RK), CPA-SRK, and GERG-2008 — against the NIST IAPWS-97 isobaric reference at constant reservoir pressure (100 bars) across the temperature range relevant to the low-enthalpy case study (15–95°C). The data points correspond to the actual block temperatures sampled along the injector–producer inter-well path at the end of the 6-months doublet operation of Case 1 (discussed later).

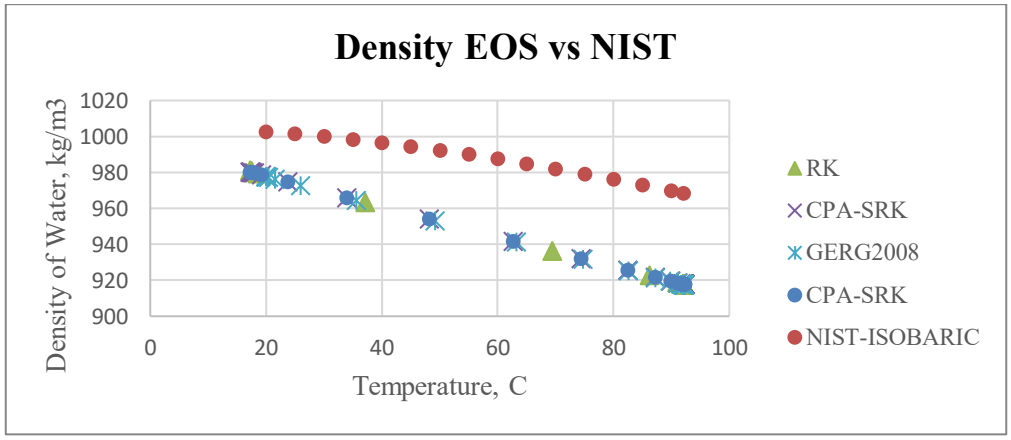

Figure 1 — Comparison of water density predictions from selected equations of state available in tNavigator® (Redlich–Kwong, CPA-SRK, GERG-2008) against the NIST IAPWS-97 isobaric reference at constant reservoir pressure (100 bara) across the temperature range 15–95°C.

Liquid water density is underpredicted in varying amounts when compared to the NIST isobaric reference using any of the three cubic and semi-empirical formulations. The biggest difference is with the RK formulation where the error is 27-30 kg/m³ at intermediate temperatures. As for the CPA-SRK, the deviation is smaller at around 23 kg/m³ in 20°C conditions, which is due to adding an association term for the hydrogen-bonding behavior of water, but the error grows to approximately 50 kg/m³ at higher temperatures of 92°C. That temperature-dependent drift is the most operationally significant finding: it shifts the thermal front predictions progressively further from reality as the temperature contrast

increases. Implementing the GERG-2008 mitigates this problem as it has a constant deviation from NIST values which is around 24-25 kg/m³ across the full cold injection range (15–35°C). It does not deviate wider at higher temperature unlike the CPA-SRK formulation.

Accordingly, GERG-2008 is the selected formulation for all Compositional Thermal model simulations as it is considered the best available model within the tNavigator® EOS library with regards to density accuracy. More importantly, it delivers a thermodynamically consistent treatment of full water-steam phase equilibrium for Case 2. This governs density, enthalpy, and vapor-liquid fugacity within a single unified framework which is crucial for an accurate representation of steam condensation, latent heat exchange, and phase transitions in the vapor-dominated scenario.

The residual 24 kg/m³ underprediction at cold injection conditions is consistent, which makes it easy is to carry forward within the simulation as a known source of uncertainty. Additionally, its effect is in one direction, leading to a slight underestimation of the volumetric contraction of the cold-water bank, and a marginally larger cold-front radius estimation compared to the true IAPWS-97 value. This is a conservative bias that does not qualitatively affect any of the conclusions.

4.3. Water Viscosity Modelling in Geothermal Reservoir Simulation

In geothermal reservoir simulations, the accurate determination of fluid viscosity is crucial because it directly dictates the fluid mobility, pressure drawdowns, and the propagation speed of the cold temperature front between the injection and production wells. tNavigator® offers several mathematical models to calculate the viscosity of the aqueous phase, ranging from simple empirical correlations to rigorous international thermodynamic standards. Which model is most appropriate depends on the specific conditions of the reservoir — particularly its temperature, pressure, and fluid composition.

4.3.1. The Grabowski Correlation

The Grabowski Correlation is the default water viscosity model used by tNavigator®'s thermal and temperature engines. It calculates water viscosity purely as an empirical function of the local fluid temperature (*tNavigator® Technical Reference Manual*, 2024).

The mathematical formulation is expressed as:

$$\mu_w = \frac{A_w}{-1 + B_w T_F + C_w T_F^2} \quad (27)$$

Where μ_w is the water viscosity, T_F is the temperature in degrees Fahrenheit, and A_w, B_w, and C_w are user-defined correlation coefficients.

However, because it depends solely on temperature and ignores pressure, Grabowski becomes unreliable wherever the two are coupled — most critically near the saturation curve, where small pressure changes drive phase transitions and the viscosity behavior of the fluid can no longer be captured by a temperature-only function.

4.3.2. The IAPWS-08 Formulation

For pure, salt-free geothermal doublets, the most rigorous and scientifically accurate viscosity model is the IAPWS-08, International Association for the Properties of Water and Steam 2008, formulation (Huber et al., 2009). This model can be forced by the simulator by activating the IAPWS08 option within VISCOPTS keyword.

Unlike empirical correlations, the IAPWS-08 formulation computes viscosity dynamically as a coupled function of both absolute temperature and density. Because fluid density is intimately linked to pressure via the EOS, this model captures how fluid mobility shifts due to the pressure gradients between the injection and production wells. The viscosity is calculated using a reference value ($\mu^* = 1.00 * 10^{-6} Pa.s$), a reference temperature ($T^* = 647.096\,K$), and a reference density ($\rho^* = 322.0\ kg.m^{-3}$) (*tNavigator® Technical Reference Manual*, 2024). In addition, this formulation ensures that the immense pressure drawdowns between the injector and production wells are physically respected. IAPWS-08 model accurately calculates the mobility of both the injected cold water and the highly compressible steam phase by coupling the density and viscosity changes instead of relying on a static empirical curve, which decreases the thermodynamic uncertainty in the propagation of the cold front.

However, the IAPWS-08 model is specifically designed for chemically pure water and steam. Therefore, its primary limitation is its weakness when the system has brines with high-salinity or dissolved non-condensable gases (such as CO2). In addition, it is slightly more computationally demanding than the Grabowski

correlation because it solves dependent viscosity variations. Thus, for a pure geothermal doublet evaluating phase-change thermodynamics, this added computational cost is necessary to ensure physical accuracy.

4.3.3. Kestin's Correlation

Kestin's Correlation, activated via the KESTIN option is a highly specialized model designed to account for the impact of dissolved salts on water viscosity.

This model calculates the viscosity of the brine (μ_b) with a pressure coefficient (β) and the specific salinity of the fluid (m, measured in g.mol/kg) (*tNavigator® Technical Reference Manual*, 2024).

The limitation of Kestin's correlation lies in its specific application to saline environments. For pure geothermal doublets devoid of salt components, utilizing this model introduces unnecessary complexity without providing any thermodynamic benefit over the IAPWS-08 standard.

4.3.4. The Slott Viscosity Model

The Slott Viscosity model is an alternative empirical correlation used primarily when the geothermal fluid contains dissolved carbon dioxide, commonly paired with the **Ezrokhi's method (21)** for density calculations.

The general form of the correlation is:

$$\mu = \frac{A}{(t + C)^B} \quad (28)$$

Where t is the temperature in degrees Celsius, and $A, B,$ and C are specific correlation coefficients B.

Yet, as mentioned for the Grabowski correlation, the Slott model is highly empirical and lacks a direct dependence on fluid density or pressure. For pure water systems without dissolved CO_2, IAPWS-08 remains a superior choice.

4.3.5. Comparison between Viscosity models

To determine which viscosity model is most appropriate for this study, a comparison was carried out across the temperature range relevant to Case 1.

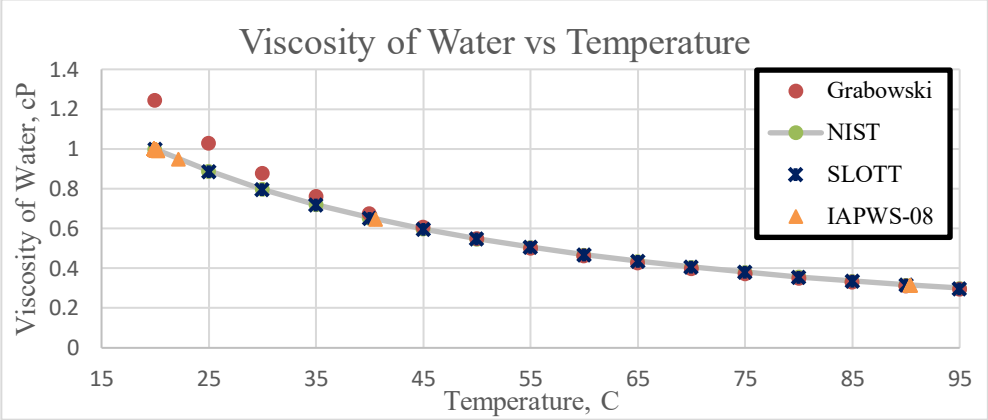

Figure 2 — Comparison of water viscosity predictions from available tNavigator® models against the NIST IAPWS-97 reference and the IAPWS-08 formulation across the temperature range 15–95°C at 100 bara.

At 20°C — the injection temperature and the single most important operating point in this study — Grabowski predicts a viscosity of approximately 1.27 cP against the NIST reference of 1.00 cP, a difference of approximately 27%. Since fluid mobility scales inversely with viscosity ($\lambda = k/\mu$), adopting Grabowski would introduce a systematic difference of 27% in near-well water mobility relative to NIST-consistent formulations, which would systematically distort the pressure transient propagation and the mobility ratio extracted from the composite well test. The inner zone — where cold injection water creates the composite signature — this discrepancy is most pronounced. Grabowski is therefore not consistent with the NIST reference standard adopted in this work and was not selected.

The Slott model and IAPWS-08, by contrast, track the NIST reference so closely that the NIST data points are largely hidden beneath both curves in Figure 2. Either model would be acceptable on accuracy grounds alone.

IAPWS-08 is adopted for all Compositional Thermal model simulations. The Slott model was set aside immediately — it is designed for CO_2-bearing geothermal brines and applying it to a pure water system would introduce composition-specific complexity that serves no purpose here. The major reason for preferring IAPWS-08 from the remaining options is that it computes viscosity as a coupled function of both temperature and fluid density, rather than temperature alone. Across the inter-well domain, pressure varies measurably between the injector and the producer, and IAPWS-08 captures the resulting density-dependent viscosity changes that a temperature-only correlation would overlook. In Case 2 this is particularly important: the viscosity must transition continuously from cold liquid water (~1.001 cP) to superheated steam (~0.015 cP) across a phase boundary, and IAPWS-08 handles this within a single formulation without any special case switching.

For Black-oil models, a table describing viscosity changes with temperature was imposed, obtained by IAPWS-08 correlation.

4.4. Rates conversion from surface to reservoir

Because both models rely on completely different thermodynamic frameworks, the simulator must use different mathematical routes to convert the surface rates into the corresponding reservoir volumes.

4.4.1. Temperature model

The Temperature model converts between reservoir and surface volumes through the empirical Formation Volume Factors read from the PVT tables — a straightforward calculation that multiplies each phase's bulk reservoir volume by the appropriate FVF to give the standard cumulative outputs reported at surface conditions. It is fast and numerically robust, but the reported volumes are only as reliable as the PVT tables themselves. As shown in §4.2.1, those tables anchor fluid density at a fixed reference temperature, so any temperature-driven density change during injection goes unaccounted for in the surface volume calculation.

4.4.2. Compositional Thermal model

The Compositional model takes a more physically complete route. Rather than reading volumes from a PVT table, it tracks the molar masses of individual chemical components throughout the reservoir and, at the point of reporting, flashes the produced moles to standard conditions via the EOS — determining how they partition between liquid and vapor before converting to surface volumes. The additional computational cost this brings also comes with an additional capability: the model can report both the energy injection total and the energy production total, quantities that the Temperature model's FVF-based framework cannot produce. For a geothermal doublet, where heat extraction efficiency over the field lifetime is the central operational question, these outputs are directly meaningful.

Chapter 5 – Case Study Definition

5.1. Introduction

This chapter defines the reservoir model and doublet geometry used throughout the study. The goal is a setup simple enough to isolate the effect of the thermal formulation choice, while still being physically representative of real geothermal conditions.

Two scenarios are considered (figure 3): Case 1, a low enthalpy liquid-dominated aquifer doublet, and Case 2, a high enthalpy vapor-dominated aquifer doublet, mimicking Larderello-Travale field's conditions. Both scenarios simulate a simplified doublet — one cold-water injector and one hot-fluid producer separated by 400 m. Cold water was injected at a fixed temperature of 20°C in both scenarios — well below the initial reservoir temperature — driving the progressive formation and advance of a thermal front centered on the injector. A Draw-down/Build-up test is performed at the injector well after months/years of operations for cooled zone extension monitoring.

Each scenario was simulated on a three-dimensional Cartesian grid in tNavigator® with both the Black-oil Temperature model and the Compositional Thermal model.

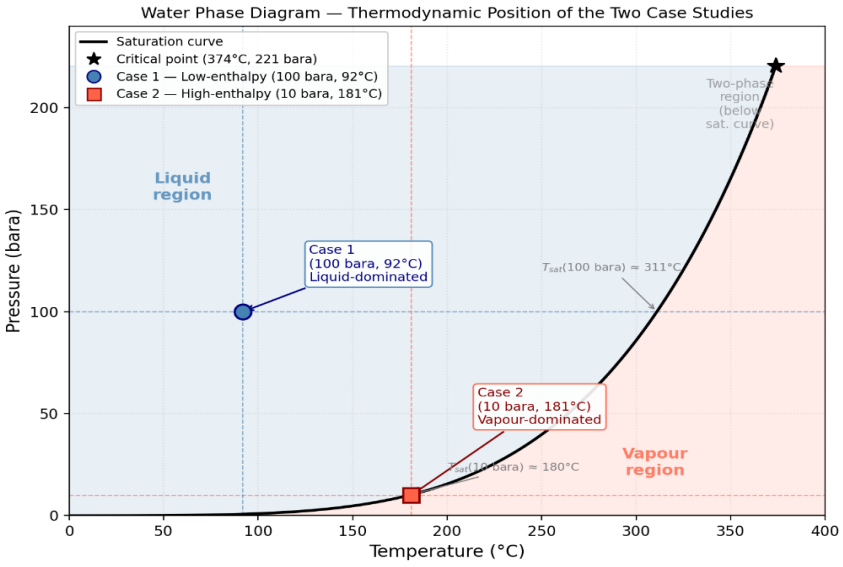

Figure 3 — Water pressure–temperature phase diagram showing the thermodynamic position of the two case studies relative to the liquid–vapor saturation curve (IAPWS-97).

5.2. Reference Reservoir Model

5.2.1. Larderello-Travale Geothermal System

The geographic location and surface infrastructure of the Larderello-Travale field, as well as its geological cross-section, are documented in the literature (Ebigbo et al., 2016; Romagnoli et al., 2010) and are not reproduced here. The principal thermo-hydraulic and operational parameters reported in the literature for the field are summarized in Table 1 and guided the selection of initial pressure and temperature conditions, thermal rock properties and fluid properties for the case studies defined in this chapter.

Table 1 — Principal thermo-hydraulic and operational parameters of the Larderello-Travale geothermal field compiled from the literature

Larderello Geothermal Field		**Shallow Reservoir**	**Deep Reservoir**
Reservoir Geometry and Well Configuration	**Heat Source (K-Horizon)**	Transition between brittle rock and ductile creep, effectively acting as an impermeable, isothermal bottom boundary. Its depth varies between 3,000 m to 4,000 m in the center of the field and drops to 8,000 m at the margins	
	Target depths	Hosted in Mesozoic carbonate-anhydrite formations 500 m-1500 m	Hosted in a fractured metamorphic basement (schists, phyllites) 2000 m-3900 m
Operating Conditions (Initial and Boundary Conditions)	**Initial Reservoir Temperature**	**220 °C-250 °C**	300 °C-350 °C 50 °C superheating
	Initial Pressure	**10 – 20 bars**	40 – 70 bars
	Injection Temperature	**~20 – 40°C**	
	Thermal Conductivity	Caprock: 2.0-2.5 W/m.K Reservoir: 2.0-2.9 W/m.K – 4.7 W/m.K (specific carbonate sequences like Burano formation)	
	Rock Heat Capacity	2.18 $MJ/m^3.K$	
	Rock Density	2780 – 2940 kg/ m^3	

5.2.2. Geological Description

The reservoir model adopted in this study uses a simplified homogeneous geometry designed for numerical sensitivity analysis. The high-enthalpy Case 2 scenario is parameterized using conditions representative of the Larderello-Travale field (Table 1, §2.3); the low-enthalpy Case 1 scenario uses conditions typical of deep sedimentary aquifer doublets.

The model consists of a geothermal doublet — one injector and one producer — completed within a homogeneous reservoir and separated by 400 meters. Both wells penetrate the full reservoir thickness and are placed symmetrically along the central axis of a 7.5 km aquifer, 60m thick. The domain is discretized with a three-dimensional Cartesian grid of 192 × 196 cells in the horizontal plane. Cell size increases progressively away from the wells toward the model boundaries (Figure 4): the wellbore region uses cells as small as 1 m × 1 m, stepping up through 2.5 m buffer cells to 10 m × 10 m in the near-well area, then to 50 m, 100 m, and 1,000 m cells toward the domain edges. Vertically, the two cases differ: Case 1 resolves the reservoir into five 12 m layers (60 m total) to capture the thermal stratification expected in a liquid-dominated system, while Case 2 uses a single 60 m layer, appropriate for the more uniform pressure and temperature conditions of a steam-dominated reservoir (Figures 3 and 4).

The principal rock thermo-hydraulic properties are identical for both cases and are summarized in Table 2. Lateral permeability is 250 mD, vertical permeability is 10 mD (a vertical-to-horizontal ratio of 0.04), and porosity is 0.20. Thermal conductivity, rock heat capacity, and rock density are assigned values consistent with the fractured carbonate-metamorphic basement of the Larderello system. The reservoir is bounded laterally and vertically by no-flow conditions, with the outer boundary placed sufficiently far from both wells to remain effectively infinite-acting over the simulation timescales considered.

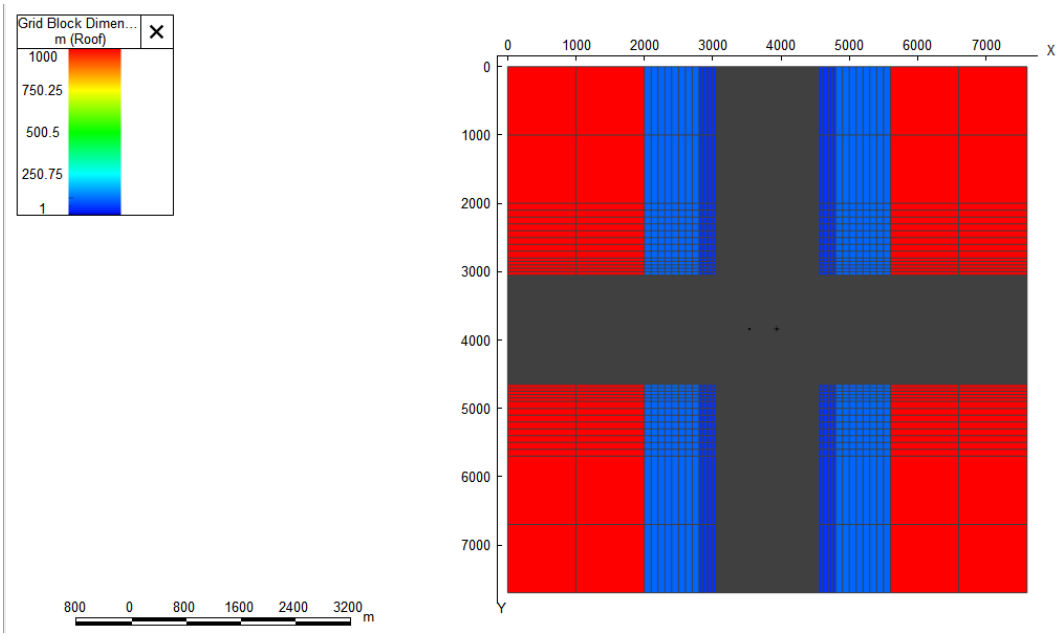

(a)

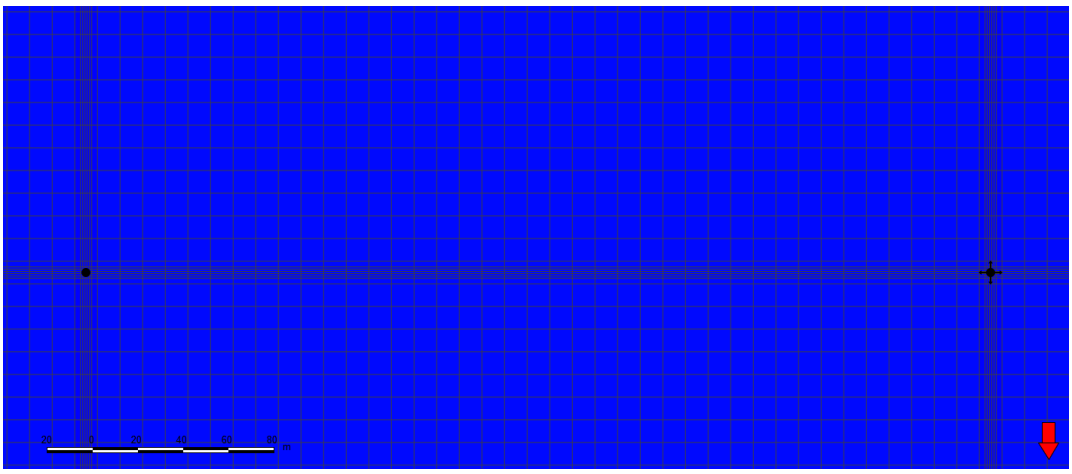

(b)

Figure 4 — Top view of simulation grid (a) and zoom of the inter-well area (b).

Table 2 — Summary of the principal reservoir properties adopted in the reference model

	Case 1 – Low Enthalpy Scenario	Case 2 – High Enthalpy Scenario
Reservoir Depth (m)	1,000	500
Reservoir Thickness (m)	60	
Number of Layers (-)	5	1
Layer Thickness (m)	12	60
Initial Temperature (ºC)	92	181
Initial Pressure (bara)	100	10
Saturation Temperature (ºC)	311	179.9
Porosity (-)	0.2	
Lateral Permeability (mD)	250	
Vertical Permeability (mD)	10	
Well Spacing (m)	400	

5.2.3. Fluid Model Configurations

Two thermal formulations were investigated for each scenario. The Temperature model (TEMP) is a temperature-dependent black-oil framework: fluid properties — density, and formation volume factor — are read from pressure-dependent PVT tables anchored at a fixed reference temperature, with no dynamic response to temperature-driven density changes or phase transitions; Conversely, viscosity dependency from temperature is accounted for by the introduction of a table (WATVISCT), calibrated against the IAPWS-08 standard. The Compositional Thermal model (COMP) calculates the fluid properties dynamically using the GERG-2008 equation of state which correctly addresses the temperature-dependent density, two-phase steam–water equilibrium, and latent heat exchange without relying on pre-tabulated values. Both formulations handle the viscosity standardized according to IAPWS-08, so any viscosity difference that appears along the inter-well path between them traces the difference in temperature distributions and not the viscosity model. This separation is what makes the inter-model comparison clean and interpretable. To ensure the results reflect model formulation effects alone, both formulations were initialized with identical reservoir geometry and rock properties; furthermore, the same operational conditions were imposed.

5.3. Case 1: Low-Enthalpy Scenario

Case 1 represents a low-enthalpy liquid-dominated geothermal doublet, parameterized to be representative of deep sedimentary aquifer systems such as the Paris Basin Dogger formation. The reservoir was set at an initial temperature of 92°C at a depth of 1,000 m and an initial pressure of 100 bara. Cold water is injected at 20°C, creating a temperature contrast of 70°C between the injected fluid and the undisturbed reservoir (Table 3). With the saturation temperature at 100 bara sitting at approximately 311°C, the domain stays more than 220°C below the boiling point at every location. The simulation is single-phase throughout with neither steam generation nor phase-change dynamics.

Both wells operate under fixed volumetric flow rates. The production rate is fixed at 3,000 sm^3/day and equals the injection rate, ensuring volumetric mass balance. This rate-controlled configuration is representative of geothermal developments where the injection–production pair can be operated symmetrically under stable, imposed volumetric constraints.

The physical setup of Case 1 is simple. Both models will see the same single-phase liquid physics; the only source of divergence between them is the density treatment, and in turn, volume factor. The Temperature model uses a fixed PVTW density referenced at 92°C, while the Compositional model computes density dynamically from GERG-2008. Cold injected water at 20°C is about 3.7% denser than the displaced reservoir water; the reservoir formation volume factor is correspondingly lower, approximately by a factor $1/1.037$. Thus, at the same surface injection rate, the cold water occupies less reservoir volume than the Temperature model assumes. Because the Temperature model reads Bw from a table anchored at the warm reservoir temperature, it assigns too large a reservoir volume to each surface cubic meter of injected cold water pushing the simulated cold waterfront further from the injector than it physically should extend.

Case 1 provides the cleanest test of this mechanism. No phase transitions, no condensation, no latent heat — just the density, compressibility, and volume-factor treatment operating in isolation, with nothing else to complicate the picture. It is the natural reference point for understanding what happens in Case 2, where multiple mechanisms act simultaneously.

Table 3 — Operating conditions of Case 1 – Low Enthalpy Scenario

Reservoir Initial Temperature (°C)	92
Reservoir Initial Pressure (bara)	100
Injection Temperature (°C)	20
Production Rate, P1 (sm^3/day)	3,000
Injection Rate, INJ (sm^3/day)	3,000
Operation Period before the well test (months)	6
Well Test Schedule	12-hour drawdown / 12-hour build-up

5.4. Case 2: High-Enthalpy Scenario

Case 2 represents a high-enthalpy vapor-dominated geothermal system, parameterized using conditions inspired by the Larderello-Travale field described in §2.3. The initial reservoir temperature is 181°C, which is superheated relative to the saturation temperature ($T_{sat} \approx 179.9$°C) at the initial reservoir pressure of 10 bara. The reservoir fluid exists entirely as single-phase superheated steam at the start of the simulation, dominating the undisturbed outer reservoir.

Cold water is injected at 20°C at a rate of 150 sm^3/day into a reservoir initially at 181°C. The producer P1 operates under an imposed drawdown of 2 bara below reservoir pressure, producing superheated steam and liquid water in response to this constraint. This configuration reflects the pressure-dependent productivity of vapor-dominated systems such as Larderello (§2.3), where steam production rates respond to the imposed drawdown rather than being directly prescribed.

Notice that cold water at 20°C has a viscosity of approximately 1.001 cP; superheated steam at 181°C has a viscosity of about 0.015 cP. That gives a mobility ratio M ≈ 0.015, roughly 22 times more extreme than in Case 1

When cold water advancing from the injector reaches the surrounding superheated steam, it triggers condensation at the phase boundary. The latent heat released in that process — approximately 2,257 kJ/kg — partially reheats the cold waterfront, slowing the outward advance of the thermal boundary relative to the fluid displacement front. Over years of operation this produces a persistent two-phase interface between the cold liquid bank and the steam reservoir beyond it.

Tracking where that interface sits, and how it evolves, requires the phase equilibrium calculations that only the Compositional Thermal model performs.

.

Table 4 — Operating conditions of Case 2 – High Enthalpy Scenario

Reservoir Temperature (ºC)	181
Initial Reservoir Pressure (bara)	10
Injection Temperature (ºC)	20
Production-Induced Pressure Drop at P1 (bara)	2
Injection Rate, INJ (sm^3/day)	150
Operation Period before the well test (years)	10
Well Test Schedule	12-hour drawdown / 12-hour build-up

Chapter 6 – Results and Discussion

This chapter covers the results of the four simulations — two thermal formulations run across two thermodynamic scenarios — together with the well test analysis and comparison between them. Two questions are addressed through discussion. How does the choice of thermal formulation affect the size and fluid properties of the cold zone as it develops during doublet operation? And does the composite radius extracted from the well test reliably reflect the actual cold-front position?

Case 1 is the simpler of the two, with inter-model differences reduced to the density, compressibility, and volume-factor treatment working in isolation. Case 2 is much harder because of the presence of steam condensation, latent heat, and two-phase dynamics which in turn, push both the simulator and the well test framework into conditions which neither was originally built for.

Section 6.1 compares the thermal front, pressure and properties profiles obtained from the numerical simulation for each formulation and scenario. Section 6.2 analyzes the pressure transient test simulated at the injector well, with Sections 6.2.1 and 6.2.2 detailing the low- and high-enthalpy cases, respectively. Finally, Section 6.2.3 provides a direct comparison between the well test scenarios, evaluating how reservoir enthalpy and fluid description impacts the diagnostic derivative.

6.1.1. Case 1 – Low-Enthalpy Scenario

6.1.1.1. 6 months Pre-Well Test Doublet Operation: Thermal Front and Pressure Field Evolution

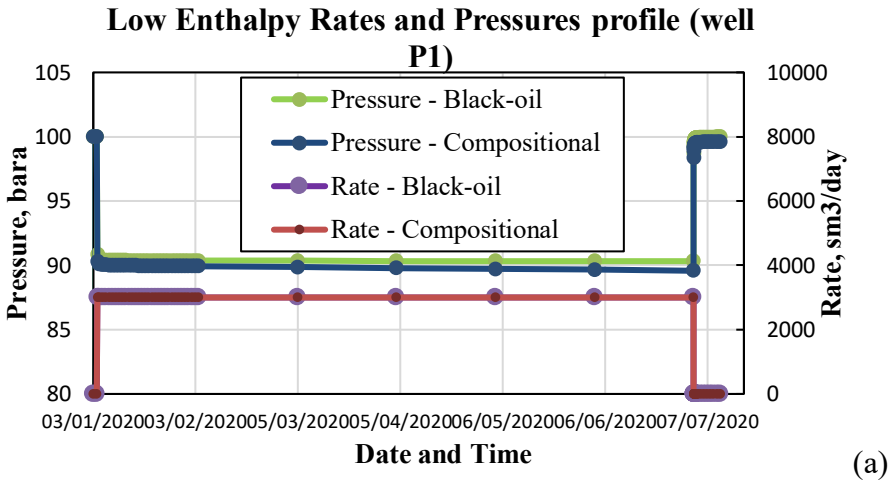

(a)

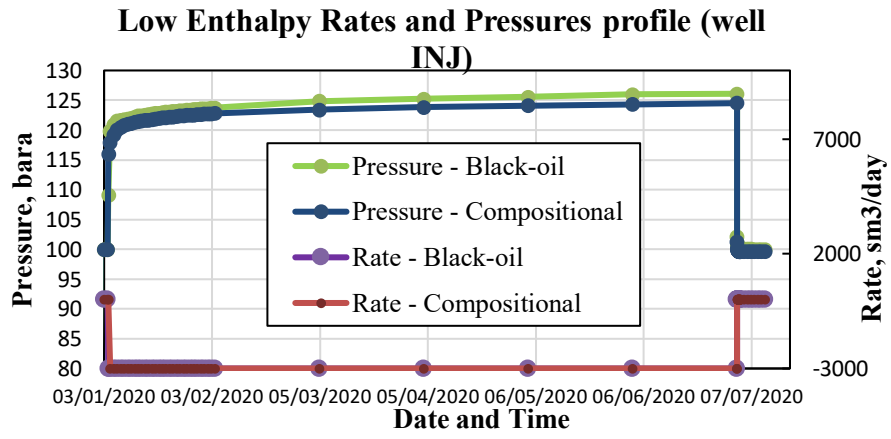

(b)

Figure 5 — Low Enthalpy Rates and Pressures Profiles *over the 180-day of doublet operation* for producer P1 (a) and injector INJ (b): *Bottom-hole pressure and water flow rate. Injection rates are negative by convention.*

Figure 5 shows the pressure and flow rate history of the doublet operations before the test was performed (6 months) for Case 1.

Before injection begins, both models run a three-day static equilibration period (1–4 January 2020) at zero flow. Both settle to a stable 100 bara — confirming that the initial conditions are consistent and that any subsequent pressure change originates from the doublet operations rather than numerical artefacts.

When injection starts at 3,000 sm^3/day, the injector BHP rises sharply. Both models jump within the first 24 hours — the Temperature model to approximately 109 bara, the Compositional model to approximately 116 bara — then continue climbing over the following weeks before levelling off around 126 bara and 125 bara respectively by the end of the first month. The 1 bara gap between them traces to the different compressibility values each formulation assigns to liquid water where the Temperature model reads $Cw = 4.5\times10^{-5}$ bar^{-1} from the PVTW table, while GERG-2008 used in the Thermal Compositional model, produces a slightly different value, which translates to a marginally different volumetric response per unit pressure gradient.

After this initial plateau, both models move upward at about 0.1–0.2 bara per month. The cold viscous water accumulating in the near-well zone gradually raises the hydraulic resistance to injection, and the BHP increases slowly to compensate.

At the same time, a rate of 3,000 sm3/day is imposed at the producer P1. This induces a pressure reduction of about 10 bars over the considered period, while slightly higher for the compositional model.

Before the test is performed at the injector, shut-in (2 July 2020) of 8 days is imposed in both wells to allow the pressure to equilibrate. Both models converge toward 100 bara — the Temperature model reaching 100.01 bara and the Compositional model settling at 99.65 bara, about 0.35 bara short at the injector. This small lag in the Compositional model is attributable to its higher effective compressibility from GERG-2008 relative to the PVTW table.

6.1.1.2.Pressure Field Evolution

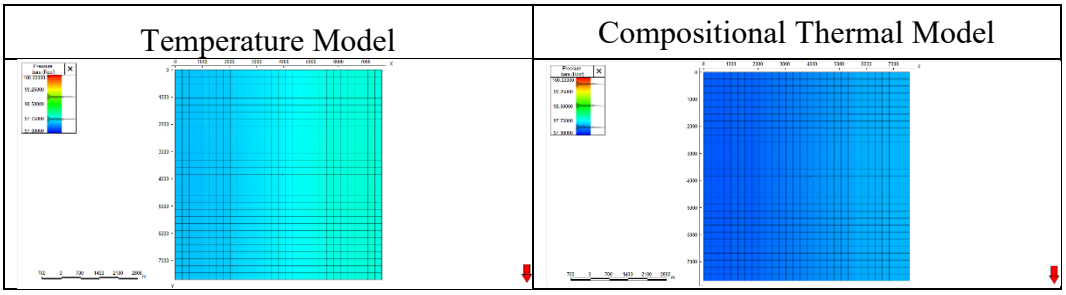

Figure 6 — P maps after 6 months. ***Color scale represents pressures from 97 bara (blue) to 100 bara (red).***

Figure 6 presents the plan-view reservoir pressure distribution at 6 months of doublet operation for both thermal formulations in Case 1.

The pressure field in both maps is uniform across the entire domain with steady state reached within the first few days of operation. The Temperature model shows pressures predominantly in the 97–99 bara range, with slightly higher values in the zone near the injector and lower ones in the zone near the producer. The Compositional Thermal model sits marginally in the lower domain-average pressure, consistent with the lower Bw at the injection face at: Bw ≈ 0.99 versus the Temperature model's 1.029 each surface cubic meter of cold water displaces slightly less reservoir volume, producing a smaller pressure response. The inter-model pressure difference across the domain is small — approximately 1 bara at the injection face — and the overall spatial distribution is essentially identical in both formulations. The steady pressure distribution visible at 6 months reflects the very high hydraulic diffusivity of liquid water. For the warm liquid outer zone of Case 1 (μ ≈ 0.317 cP at 92°C, $C_t \approx 4.5\times10^{-5}$ bar^{-1}):

$$\eta_{water} = \frac{k}{\emptyset \times \mu_{water} \times c_t} = \frac{250}{0.20 \times 0.317 \times 4.5 \times 10^{-5}} \approx 8.76 \times 10^7\ mD/(cP \cdot bar)$$

This is approximately 100 times higher than the steam diffusivity of Case 2 (~8.33×10^5 mD/(cP·bar)). In a slightly compressible liquid-dominated system, pressure disturbances propagate across the entire domain within the first few days of doublet operation. By 6 months the system is already at steady state, governed by the steady 3,000 sm³/day injection and production rates. Because the background pressure is steady throughout the 6 months doublet operation, the 12-hour build-up in Case 1 probes the near-well composite zone in effectively infinite-acting conditions.

The pressure investigation radius during the 12-hour test (~1,000 m, based on

$r_{inv} \approx 0.032 * \sqrt{k * \frac{t}{\phi * \mu * c_t}}$) remains within the model boundaries (~3,500–4,000 m).

6.1.1.3.Thermal Front Evolution

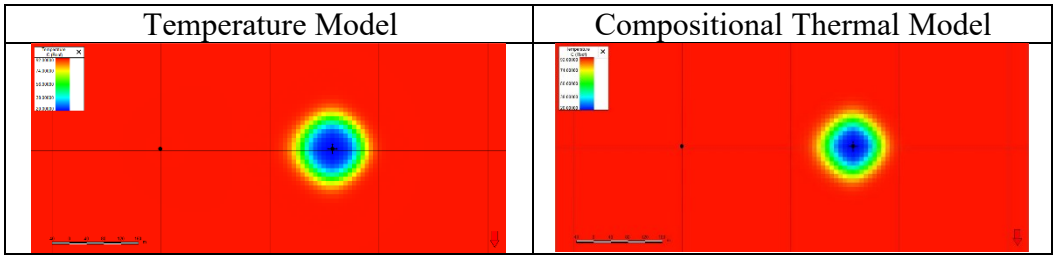

Figure 7 — T maps after 6 months of doublet operation. ***Color scale represents temperatures from 20°C (blue) to 92°C (red)***

Figure 7 shows the plan-view temperature at the end of the 180-day injection period. Both color scales are in the same range (20.0–92°C).

Both maps show a circular thermal plume around the injector with near-perfect radial symmetry, exactly what a homogeneous isotropic reservoir under uniform permeability should produce. The clearest difference is the spatial extent of the fully flushed cold-water bank (the blue zone core): in the Temperature model, this nominal cold zone radius reaches approximately 60 m, while in the Compositional model, the equivalent cold front sits 10 m closer at 50 m.

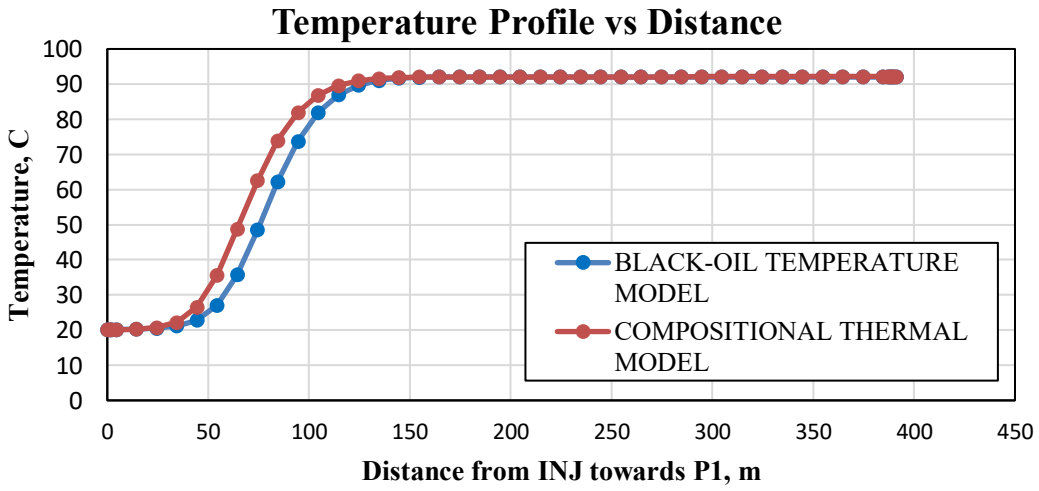

Figure 8 — Case 1 (Low-Enthalpy, 100 bara / 92°C): ***Temperature profile along the sampled INJ–P1 inter-well path at the end of the 6 months doublet operation.***

Figure 8 gives the temperature along the 391 m sampled inter-well path at the end of the injection period — the quantitative version of what the plan-view maps show spatially.

Away from the injector by about 40 m, both models superpose where the near-wellbore zone is fully flushed to the injection temperature of 20°C in both cases. The profiles then part: the Temperature model's cold front extends further, and the divergence grows until it peaks at 74.5 m, where the two curves are 14°C apart — 48.5°C for the Temperature model against 62.5°C for the Compositional model. From about 145 m onward both reach back to the undisturbed reservoir temperature.

Note that while the maximum mathematical temperature divergence between the two profiles occurs further out in the transition zone gradient at 74.5 m (where a 14°C delta is observed), the primary focus for the well test interpretation remains strictly on the 60 m and 50 m core radii, as these define the high-viscosity thermal bank boundary that triggers the composite pressure transient signature.

6.1.1.4.6-Months Doublet Operation: Properties Profiles

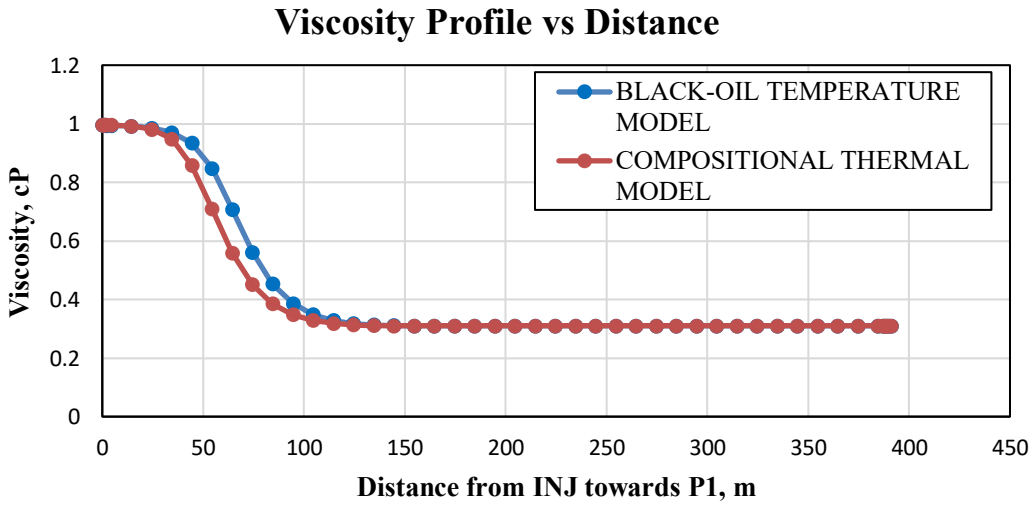

Figure 9 — Case 1 (Low-Enthalpy, 100 bara / 92°C): ***Water viscosity profile along the sampled INJ–P1 path at the end of 6 months doublet operation.***

The viscosity profile follows the temperature one. Figure 9 shows viscosity along the sampled inter-well path. Since both models use the same standard viscosity values, every difference here has the same origin as the differences in Figure 8 — it is the temperature profile translated through the μ(T) function.

In the cold near-well zone (0–35 m) both models return ~0.995 cP. Beyond ~145 m both converge to 0.317 cP at reservoir temperature. The largest viscosity gap between the two models appears at 64.5 m rather than at the 74.5 m temperature

peak, because the μ(T) curve is steepest in the 30–70°C range, where the same temperature gap translates into a larger viscosity difference. At that point the Temperature model reads 0.707 cP against the Compositional model's 0.559 cP, representing a 26.5% gap.

This has a direct consequence for the well test. The Temperature model places a high-viscosity inner zone roughly 10 m further from the injector than the Compositional model does, producing a wider low-mobility annulus creating a measurably different composite derivative signature.

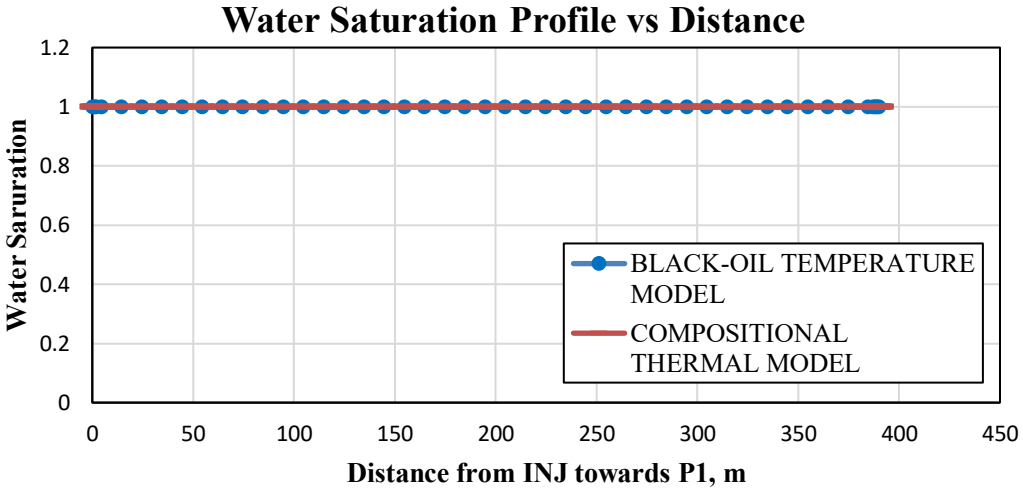

Figure 10 — Case 1 (Low-Enthalpy, 100 bara / 92°C): ***Water saturation profile along the sampled INJ–P1 path at the end of 6 months doublet operation.***

Figure 10 shows Sw = 1.0 at every grid block in both models. This is exactly what the initial conditions predict: with the saturation temperature at 311°C and the maximum domain temperature only ~92°C, the reservoir sits more than 220°C below the boiling point at every location. Which means that steam generation is thermodynamically impossible anywhere in Case 1.

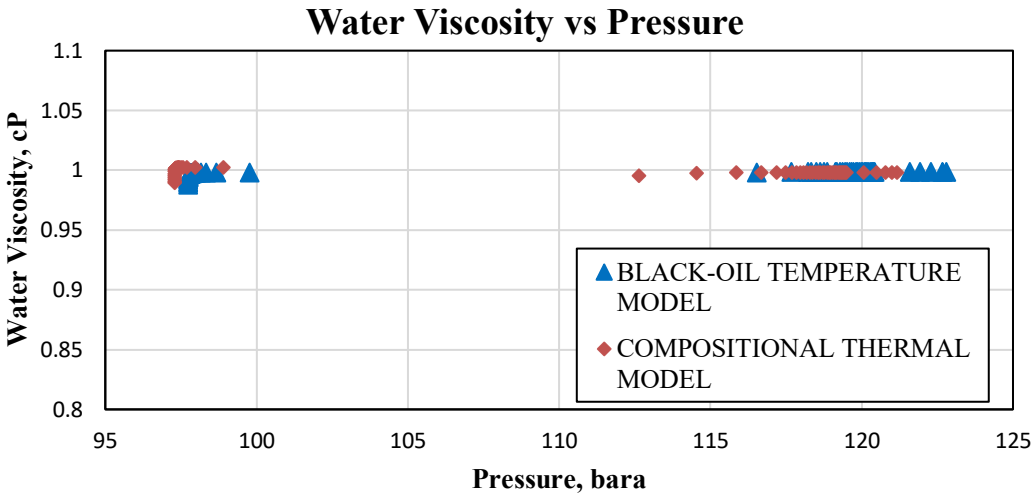

Figure 11 — Case 1 (Low-Enthalpy, 100 bara / 92°C): ***Water viscosity at the injector block plotted against bottom-hole pressure throughout 6 months doublet operation.***

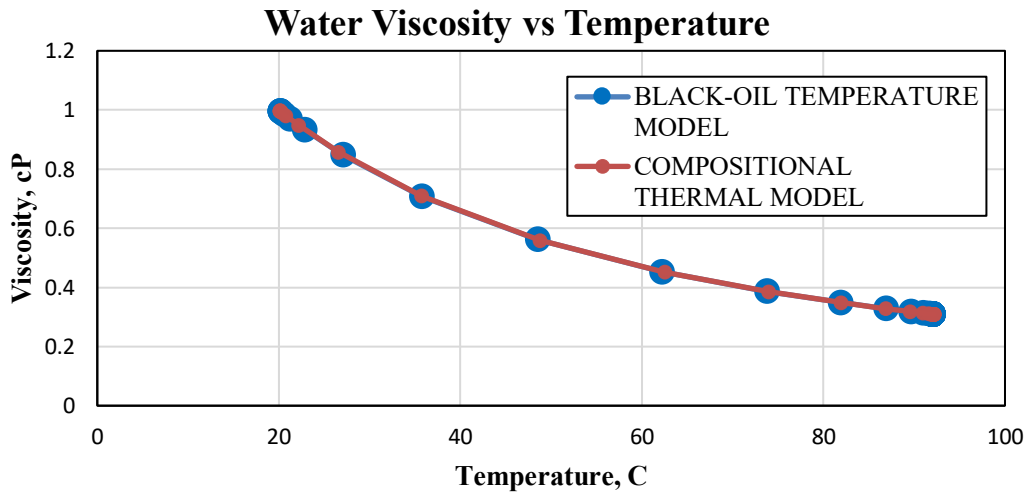

Figure 12 — Case 1 (Low-Enthalpy, 100 bara / 92°C): ***Water viscosity against temperature for grid blocks along the sampled INJ–P1 path at the end of 6 months doublet operation.***

Figures 11 and 12 establish the same core point: viscosity in both models is controlled entirely by local temperature only through IAPWS-08 viscosity table. Figure 11 plots the viscosity at the injector block plotted against BHP over the 6 months doublet operation with a negligible variation over the full 16 bara injection range. Pressure plays no role. Figure 12 then confirms the picture for all blocks along the sampled inter-well path: all data points from both models collapse onto a

single smooth μ(T) curve with no separation between the two formulations at any temperature.

The 26.5% peak viscosity difference in Figure 9 is not a viscosity-model problem, but an entirely temperature-distribution problem. The Temperature model places its cold zone 10 m further from the injector, and because it is still in the steep part of the μ(T) curve at that location, the viscosity gap looks large. The root cause lies in the density and volumetric treatment shown in Figure 14.

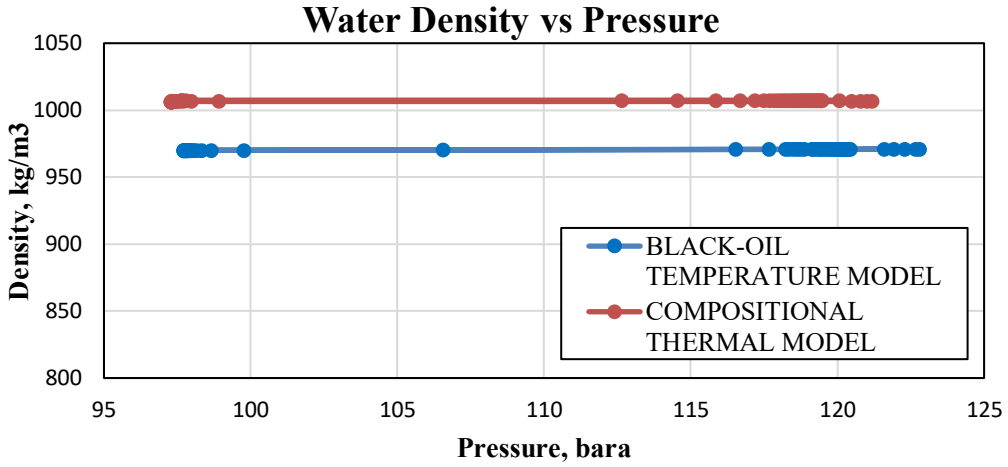

Figure 13 — Case 1 (Low-Enthalpy, 100 bara / 92°C): ***Water density at the injector block against bottom-hole pressure over the 6 months geothermal doublet operation.***

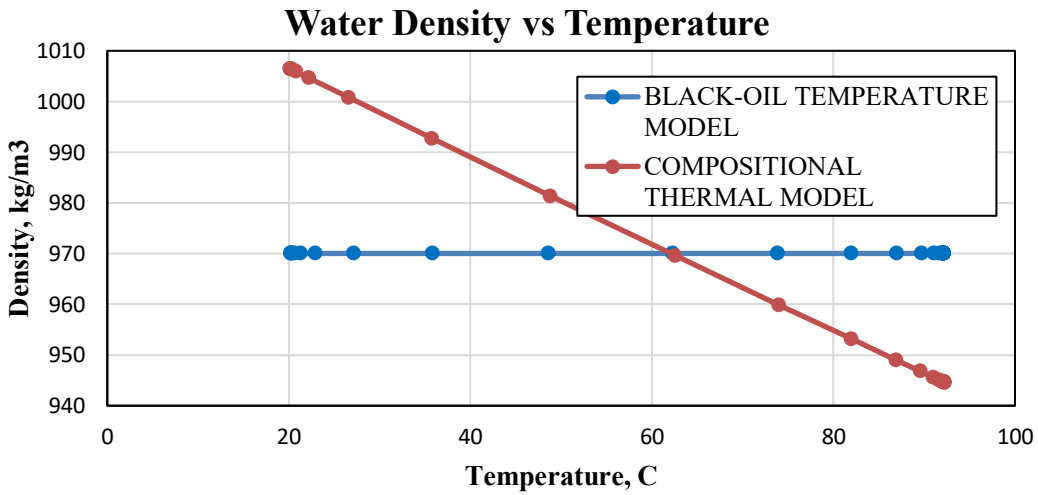

Figure 14 — Case 1 (Low-Enthalpy, 100 bara / 92°C): ***Water density against temperature for grid blocks along the sampled INJ–P1 path at the end of the geothermal doublet operation.***

Figure 13 makes two points immediately. The Compositional model (red) and Temperature model (blue) occupy separate horizontal bands — ~1,007 kg/m³ and

~970 kg/m³ respectively — with a persistent 37 kg/m³ (3.7%) gap that does not close at any pressure. Within each band, density varies by less than 0.07% over the full 16 bara injection range. For the compositional model, changes of density with pressure are irrelevant, while a non-negligible change with temperature is observed (Figure 14). Conversely, the black-oil temperature model does not account for temperature changes in density.

The same trends with temperature are observed for the formation volume factor (Figure 15).

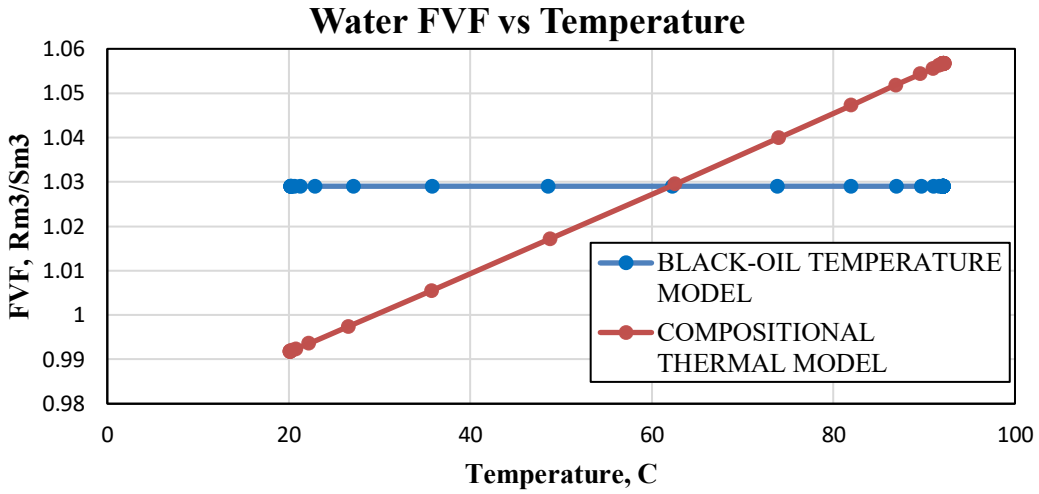

Figure 15 — Case 1 (Low-Enthalpy, 100 bara / 92°C): ***Water formation volume factor (Bw) against temperature for grid blocks along the sampled INJ–P1 path at end of the geothermal doublet operation.***

Since $B_w = \frac{\rho_{sc}}{\rho_{res}}$, every density difference maps directly to a Bw difference. The Temperature model produces a flat Bw = 1.029 rm³/sm³ across the full 20–92°C temperature range, while the Compositional model increases from Bw ≈ 0.99 at 20°C (cold water is slightly denser than the surface reference) to Bw ≈ 1.055 at 92°C (thermally expanded warm water). The crossover at ~62–65°C falls at the same temperature as the density crossover in Figure 15, as expected.

For the same surface injection rate of 3,000 sm³/day, tNavigator® computes a reservoir displacement rate of 3,000 × 1.029 = 3,087 rm³/day for the Temperature model and 3,000 × 0.99 = 2,970 rm³/day for the Compositional Thermal model in the cold zone. That 3.9% overestimation of reservoir volumetric displacement contributes to pushing the Temperature model's cold front further from the injector. Since the swept region is approximately cylindrical, the Bw difference alone accounts for a radial shift of only √1.039 ≈ 2% (1–1.5 m); the remaining gap arises from the combined effect of the different compressibility and temperature-

dependent density treatments in the two formulations, which also alter the energy balance and the resulting thermal retardation.

Table 5 — Case 1 (Low-Enthalpy, 100 bara / 92°C): Comparison of thermal front propagation between the Temperature model and the Compositional Thermal model at the end of the 6-month geothermal operation.

Model	Temperature-dependent Black Oil Model	Compositional Thermal model
Radius of the inner zone (m)	60	50
Temperature of the inner zone (^oC)	31.876	31.58805
Viscosity of water in the inner zone (cP)	0.775	0.776
Formation Volume Factor of water at inner-zone average temperature, rm3/sm3	1.029	1.002
Density of water in the inner zone (kg/m^3)	970	996.37
Effective outer zone viscosity μ (cP)	0.317	0.317
Mobility ratio M	0.33	0.35
Pi from Kappa (bara)	100.011	99.649

6.1.2. Case 2 – High-Enthalpy Scenario

In this scenario, due to the low initial pressure, doublet operations are characterized by low rates. As a consequence, a longer time simulation was performed in order to see the development of the cooled zone, reaching a radius of 50 m (TEMP) and 60 m (COMP) in about 10 years.

6.1.2.1.10 years Pre-Well Test Doublet Operation: Thermal Front and Pressure Field Evolution

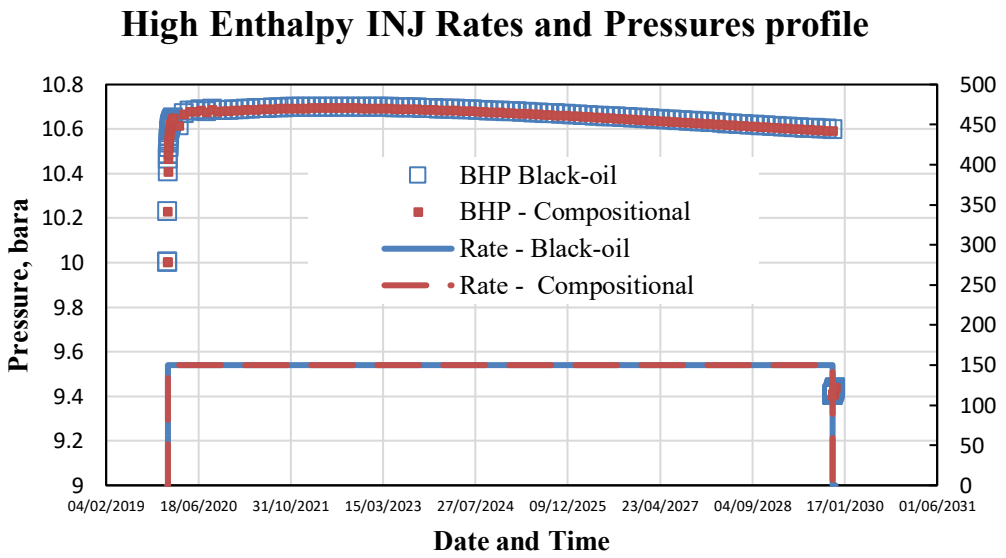

(a)

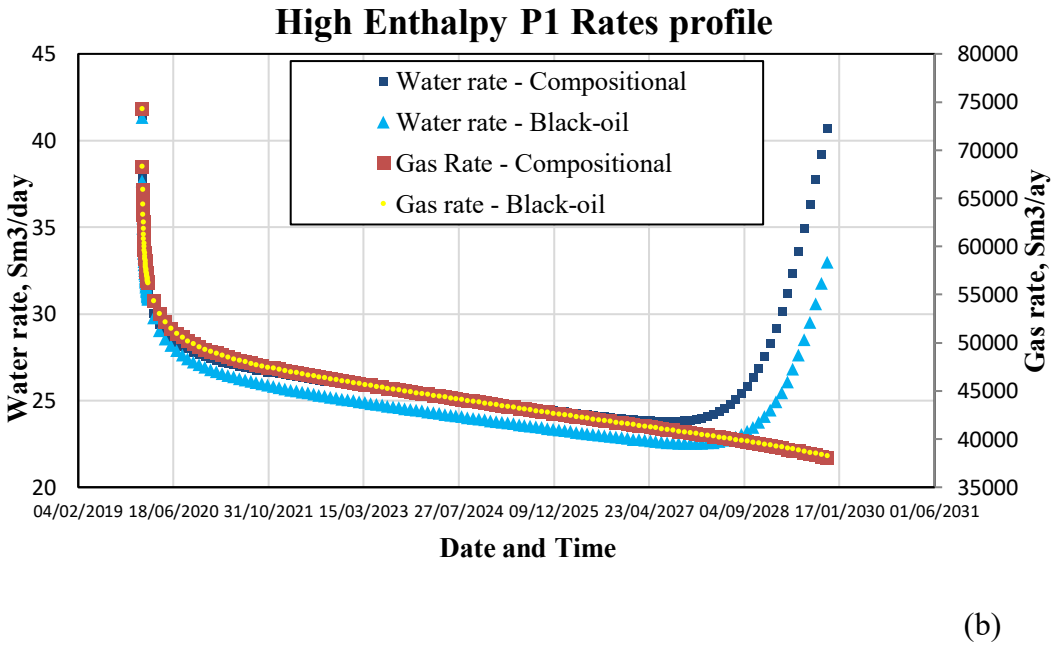

(b)

Figure 16 — Case 2 (High-Enthalpy, 10 bara / 181°C): ***Bottom-hole pressure and liquid rate history at the injector (INJ) and producer (P1) over the ten-year doublet operation period.***

Figure 16 shows the pressure and fluid rate history for Case 2 over the full ten-year operation period.

When cold-water injection begins at 150 sm^3/day, the injector BHP climbs above the initial 10 bara in both models, settling around 12–13 bara within the first timesteps. The Temperature model shows a noticeably larger initial pressure which is a direct consequence of its Bw = 1.125, which assigns 13.6% more reservoir volume to each surface cubic meter of cold water and drives a proportionally stronger near-well pressure response (Figure 16a).

Both models then drift slowly upward over the following decade. The process is gradual: as cold water progressively displaces steam in the near-injector pore space, the dominant fluid shifts from highly compressible steam to slightly compressible liquid water, and effective system compressibility falls. Smaller compressibility means the same injection volume produces a larger pressure rise. The Compositional model tracks this more accurately through dynamic phase equilibrium calculations — and consequently sits at slightly lower BHP than the Temperature model throughout the ten-year period.

The producer P1 (Figure 16 b) operates under a fixed ΔP of 2 bara revealing a stable P of 8 bara throughout the ten-year period, decreasing slightly over time as cumulative steam condensation around the injector gradually reduces the average reservoir pressure. Being the scenario steam-dominated but characterized by the contemporary presence of water and steam, appreciable rates of both liquid water and steam are produced. Steam rate is the same for both models, while appreciable differences are observed in water rates. The rate divergence between the two models grows with time and is an expression of the phase-handling differences shown in the saturation profiles of Figures 20 and 21.

$$\eta_{steam} = \frac{k}{\emptyset \mu_{steam} c_{steam}} = \frac{250}{0.20 \times 0.015 \times 0.10}$$
$$\approx 833{,}000\ mD/(cP \cdot bar)$$

6.1.2.2.Thermal Front Evolution

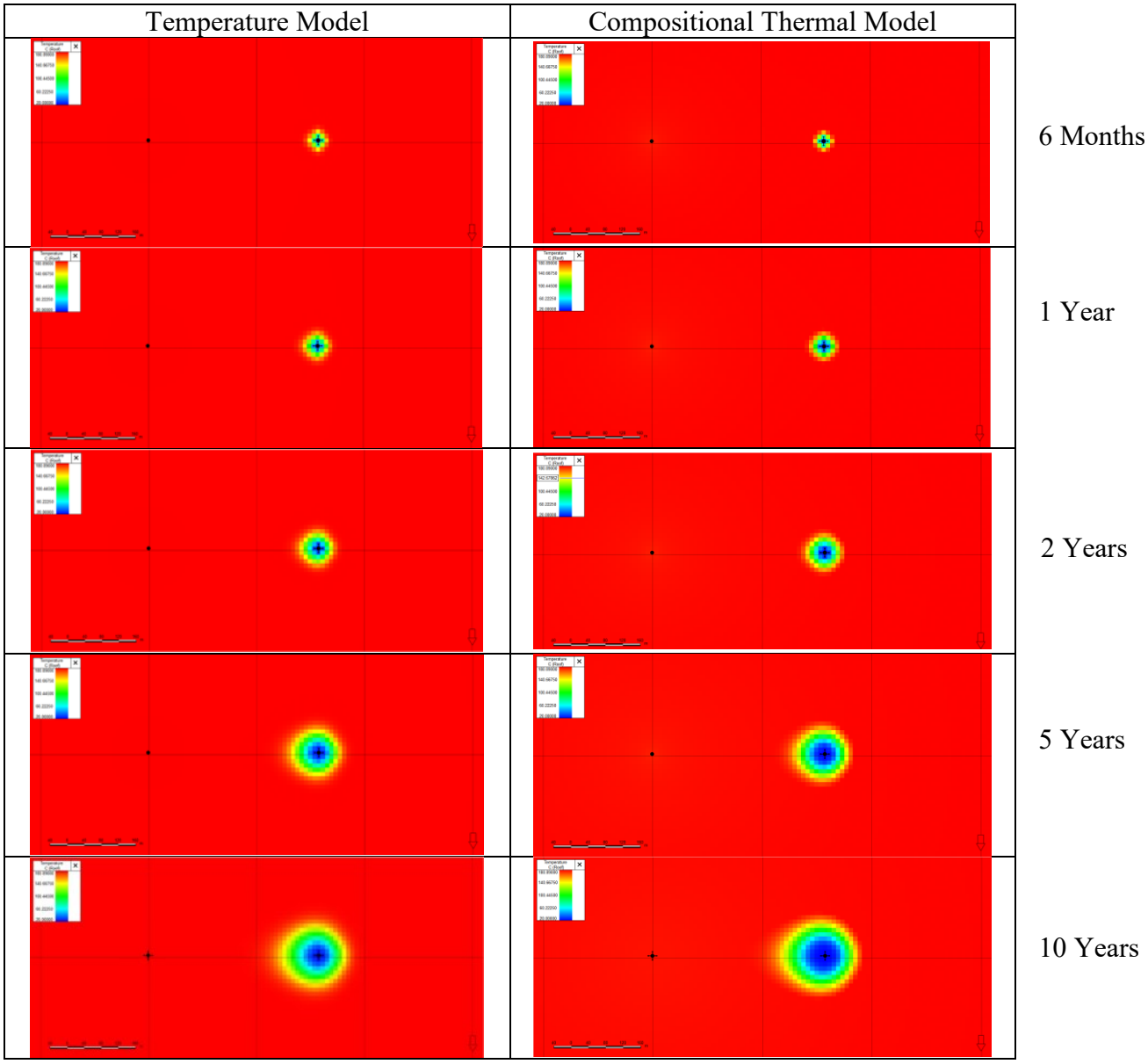

Figure 17 — T maps at 6 months, 1 year, 5 years, and 10 years doublet operation. ***Color scale represents temperatures from 20°C (blue) to 180.89°C (red).***

Table 6 – Case 2 (High-Enthalpy, 10 bara / 181°C): Comparison of the cold-zone extension at each snapshot for both formulations.

Time	TEMP cold-zone radius	COMP cold-zone radius	Difference
6 months	10 m	10 m	0 m
1 year	10 m	10 m	0 m
2 years	20 m	20 m	0 m
5 years	30 m	40 m	COMP > TEMP by 10 m
10 years	50 m	60 m	COMP > TEMP by 10 m

The cold thermal front advances extremely slowly. As Figure 17 (panels a and b) shows, after 6 months and 1 year the cold zone radius is only 10 m in both models — both formulations are in complete agreement at this stage. By 5 years the Temperature model cold zone reaches 30 m and the Compositional Thermal model 40 m. By 10 years the Temperature model reaches 50 m and the Compositional Thermal model 60 m.

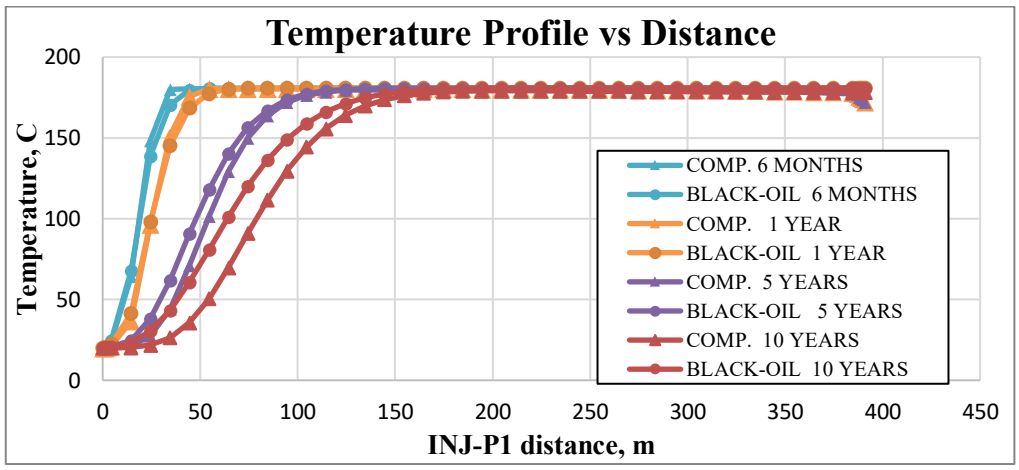

(a)

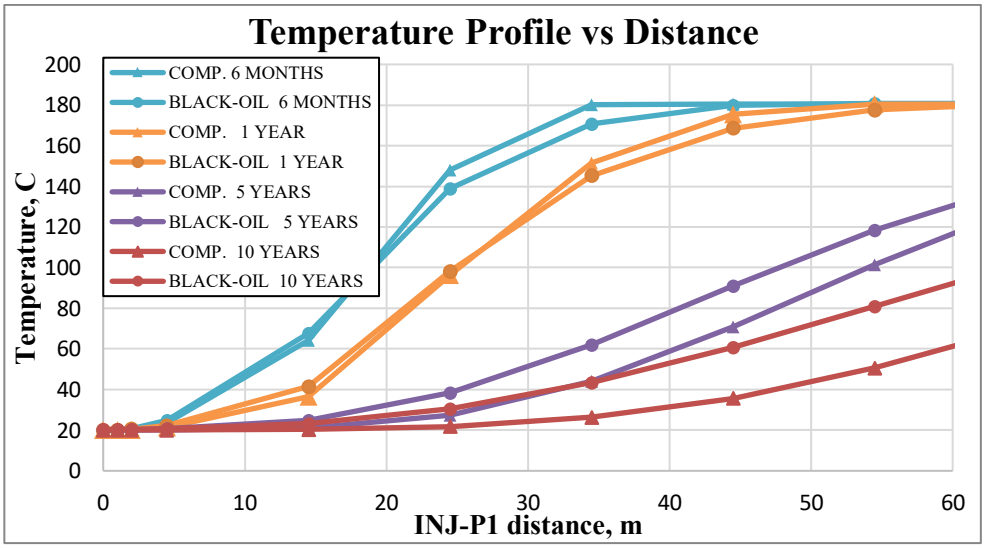

(b)

Figure 18 — Case 2 (High-Enthalpy, 10 bara / 181°C): Temperature profiles along the sampled INJ–P1 inter-well path at 6 months, 1 year, 5 years, and 10 years doublet operation. ***Panel (a) shows the sampled INJ-P1 inter-well path; panel (b) shows an enlarged view of the near-injector zone (0–60 m) to resolve the inter-model differences at the advancing cold front.***

6.1.2.3.10-Years Doublet Operation: Properties Profiles

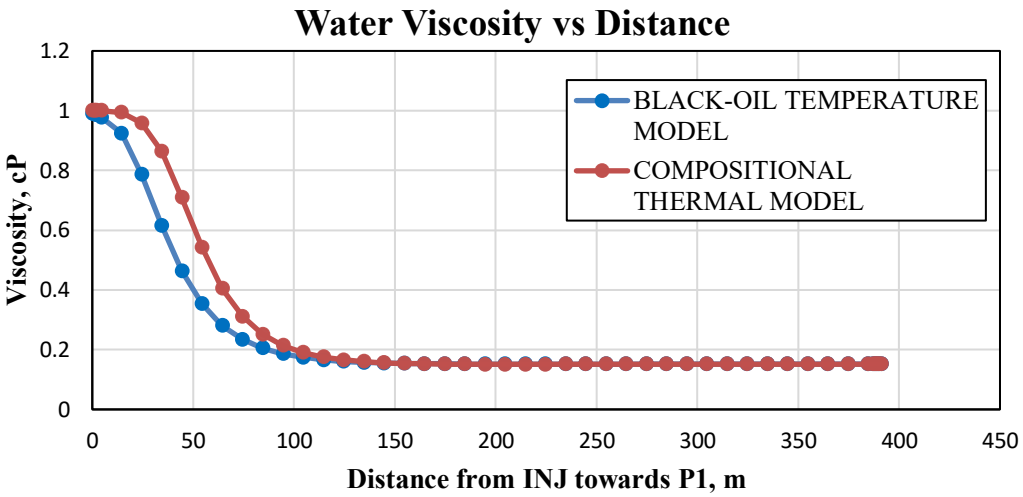

Figure 19 — Case 2 (High-Enthalpy, 10 bara / 181°C): ***Water viscosity profile along the sampled INJ–P1 path at the end of the 10-year doublet operation.***

Figure 19 shows the water viscosity distribution along the 391 m sampled inter-well path at the end of the 10-year doublet operation. Since both models use the same temperature dependent-viscosity values, any difference between the two curves is entirely a consequence of the temperature profiles established in the thermal maps above and not a difference in how viscosity is modelled.

Close to the injector both models return the same viscosity — the wellbore block has been fully cooled to 20°C in both, and since they share the same viscosity values, μ(T) is identical at that temperature of ~1.001 cP. Through the intermediate zone out to roughly 150 m, the Compositional model plots slightly higher than the Temperature model. The reason is straightforward: the Compositional model predicts a larger cold zone, so at any given radial distance it is still in colder — and therefore more viscous — territory than the Temperature model at the equivalent location. Beyond about 150 m both curves converge to a plateau of 0.13–0.15 cP — the liquid water viscosity at near-saturation conditions from the standard IAPWS-08 viscosity value.

One aspect that is easy to miss but is critical for the well test interpretation: the far-field plateau of 0.13–0.15 cP is not the outer-zone viscosity that should be used in the Kappa radial composite model. That value represents liquid water near the saturation temperature — but the far field of Case 2 is superheated steam. The steam viscosity at 181°C and 10 bara, taken from IAPWS-08, is μ_steam = 0.015 cP, roughly ten times lower. This gives the mobility ratio M = 0.015/1.001 = 0.0150 used in the Kappa analysis.

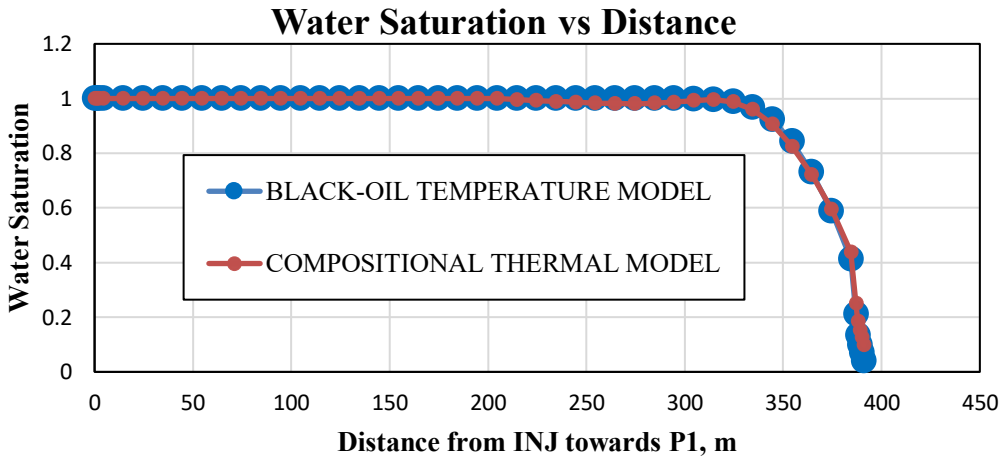

Figure 20 — Case 2 (High-Enthalpy, 10 bara / 181°C): ***Water saturation profile along the sampled INJ–P1 path at the end of the 10-year doublet operation.***

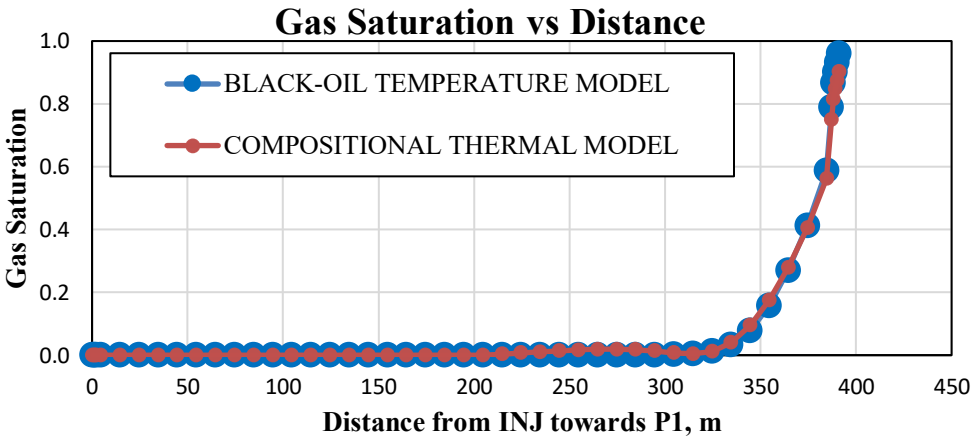

Figure 21 — Case 2 (High-Enthalpy, 10 bara / 181°C): ***Gas (steam) saturation profile along the sampled INJ–P1 path at the end of the 10-year doublet operation.***

Figure 21 shows gas saturation along the sampled inter-well path. Notice that in the transition zone, saturation values significantly differ in the two approaches. Black-oil framework cannot account for phase changes in the transition zone.

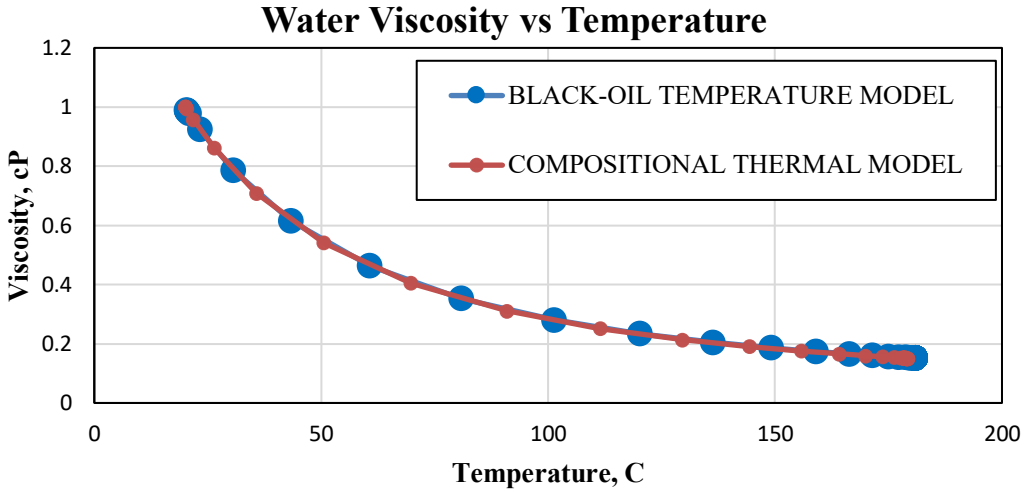

Figure 22 — Case 2 (High-Enthalpy, 10 bara / 181°C): ***Water viscosity against temperature for grid blocks along the sampled INJ–P1 path at the end of the 10-year doublet operation.***

Figure 22 shows the viscosity model from that of the spatial temperature distribution. All data points from both models collapse onto a single smooth μ(T) curve with no systematic offset between the two model families at any temperature. Both formulations use the same IAPWS-08 reference, so this result is expected — but it is still useful as confirmation that every inter-model viscosity difference observed in the spatial profile of Figure 19 is geometric in origin rather than a property difference.

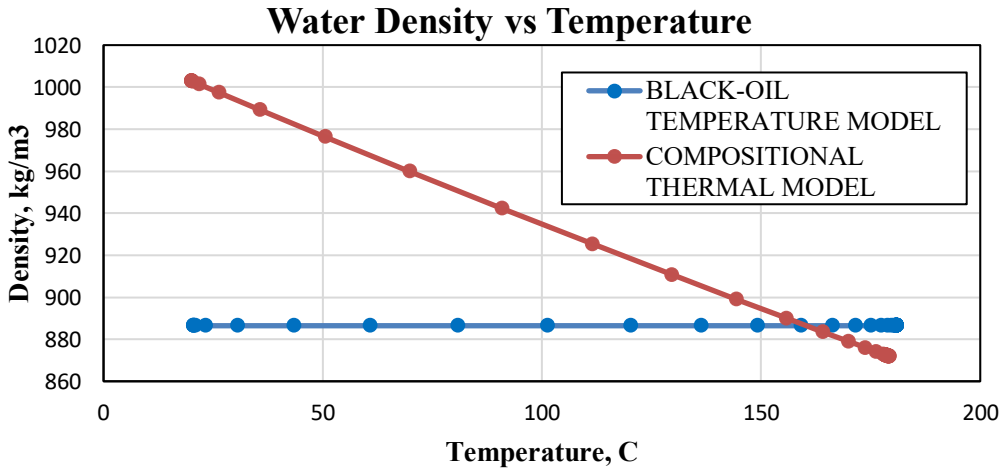

Figure 23 — Case 2 (High-Enthalpy, 10 bara / 181°C): ***Cross plot of water density against temperature for grid blocks along the sampled INJ–P1 path at the end of the 10-year doublet operation.***

Figure 23 compares the density trends with temperature for Case 2 scenario. The Temperature model produces a horizontal line at 886 kg/m³ across the entire

20–180.89°C range at the PVTW reference anchored at 181°C, while the Compositional Thermal model gives a monotonically decreasing curve from ~1,002 kg/m³ at 20°C down to ~886 kg/m³ at the saturation temperature of 179.9°C via GERG-2008. The architecture is identical to Case 1 with a different scale.

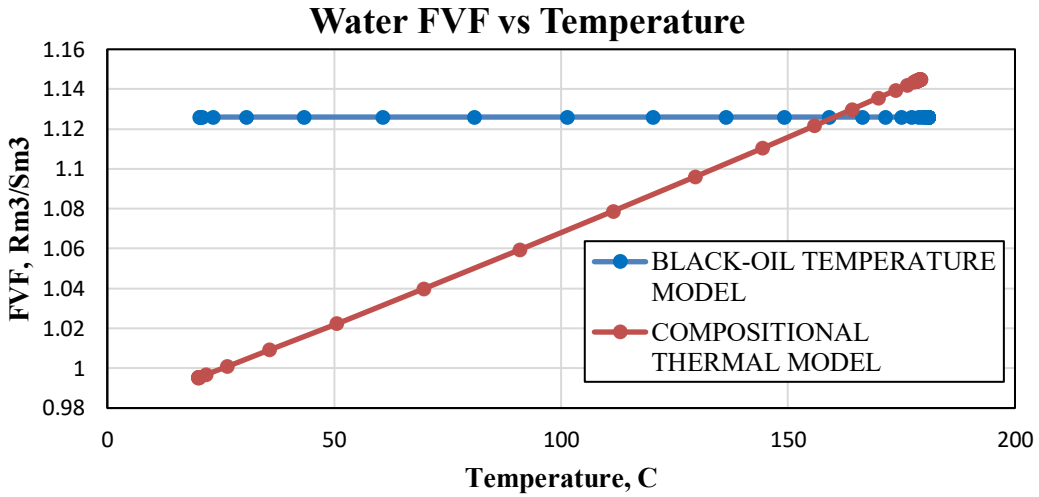

Figure 24 — Case 2 (High-Enthalpy, 10 bara / 181°C): ***Cross plot of water formation volume factor (Bw) against temperature for all grid blocks along the sampled INJ–P1 inter-well path at the end of the 10-year doublet operation.***

Since Bw = ρ_SC/ρ_res, the density gap between the two formulations carries straight through into a Bw gap as already mentioned. The Temperature model holds Bw = 1.125 rm³/sm³ at every block regardless of local temperature, referenced at the initial reservoir condition of ~181°C. The Compositional Thermal model instead tracks the actual fluid state, rising from Bw ≈ 0.99 at 20°C to Bw ≈ 1.12–1.14 at 170–175°C. At the injection face, the gap is at its largest: 13.6%, roughly four times the 3.6% seen in Case 1, where the temperature contrast between injection and reservoir is smaller.

The numbers follow directly from the flow equations. At 150 sm³/day surface injection, the Temperature model computes a reservoir displacement of 150 × 1.125 = 168.75 rm³/day while the Compositional model computes 150 × 0.99 = 148.5 rm³/day. Left to act alone, this Bw difference would push the Temperature model's cold front about 4 m further out on a ~60 m base radius, but the Compositional model ends up with the larger cold zone, by 10 m. The condensation dynamics, phase-dependent compressibility, and latent heat exchange that the Compositional model captures collectively outweigh the Bw-driven volumetric advantage of the

Temperature model, flipping the ordering seen in Case 1. The Temperature model, lacking any representation of these mechanisms, cannot predict this reversal.

6.2. Injector Well Test Analysis

After the doublet operation, both wells are shut in for a few days to let the pressure come back to the initial value. Then, a drawdown-build-up test is simulated at the injector well.

The well test consists of a 12-hour controlled production period at the injector followed by a 12-hour shut-in.

Pressure and rate data from tNavigator® were exported to Kappa Ecrin (Saphir module) for interpretation using a radial composite reservoir model.

The radial composite model used in Kappa Ecrin represents the reservoir as two concentric zones with distinct and uniform fluid mobilities, separated by a sharp circular boundary at radius Ri. The inner zone ($0 \leq r \leq Ri$) contains the cold-water bank of cold injected water at the injection temperature of 20°C and is characterized by inner-zone viscosity μ_{inner} and mobility $\lambda_1 = \frac{k}{\mu_{inner}}$. The outer zone ($r > Ri$) contains the undisturbed reservoir fluid at the initial reservoir temperature and is characterized by outer-zone viscosity μ_{outer} and mobility $\lambda_2 = \frac{k}{\mu_{outer}}$. The mobility ratio $M = \lambda_1/\lambda_2 = \frac{\mu_{outer}}{\mu_{inner}}$ quantifies the contrast between the two zones.

The fitted parameters are wellbore storage coefficient (C), skin factor (S), composite radius (Ri), mobility ratio M = μ_outer/μ_inner, and diffusivity ratio $D = \frac{\left(k.\frac{C_t}{\mu}\right)_{inner}}{\left(k.\frac{C_t}{\mu}\right)_{outer}}$. Permeability was held fixed at k = 250 mD throughout. As a consequence, the first stabilization, indicative of the cooled zone, allows us to assess the "average" viscosity, and consequently temperature, of the cooled zone and its radial extension. The mobility ratio, obtained from the position of the second stabilization, is representative of the viscosity ratio between undisturbed zone, at reservoir initial temperature, and cooled zone. For Case 1, the diffusivity ratio D was set equal to M, consistent with the near-equal compressibility of liquid water at different temperatures in both zones. For Case 2, this equality does not hold — steam compressibility at 10 bara (~0.10 bar^{-1}) is approximately 2,000 times higher than cold water compressibility (~4.5×10^{-5} bar^{-1}), so D was left as a free parameter. Initial pressure Pi was fixed in Kappa to the tNavigator® equilibrium BHP recorded at the end of the doublet operation for each model separately — 100.011 bara for Case 1 TEMP, 99.649 bara for Case 1 COMP, 9.44 bara for Case 2 TEMP, and 9.76 bara for Case 2 COMP.

6.2.1. Case 1 – Low-Enthalpy Scenario

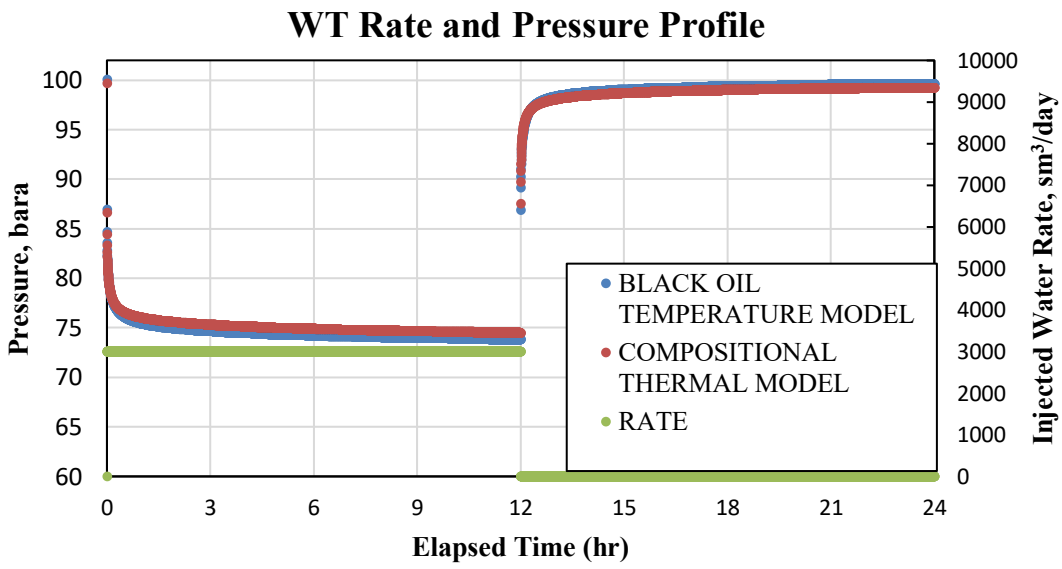

Figure 25 — Case 1 (Low-Enthalpy, 100 bara / 92°C): ***Bottom-hole pressure and water rate history at the injector well (INJ) during the 12-hour production / 12-hour shut-in well test.***

Figure 25 shows the injector BHP and water rate during the 12-hour drawdown / 12-hour build-up well test for Case 1.

When the injector reverses from cold-water injection to production at 3,000 sm³/day, the BHP drops sharply from the plateau established at the end of the 6-month period of doublet operation. Both models show an immediate pressure decline with a consistent inter-model offset throughout the drawdown — the Temperature model recording slightly higher BHP than the Compositional model at every timestep, reflecting the slightly higher reservoir pressure established during the doublet operation by the Temperature model's larger Bw, which persists as a residual offset at the start of the well test. The water rate holds steady at 3,000 sm³/day throughout.

At shut-in (43,200 s), the BHP rises in both models as the pressure transient propagates outward through the composite zone. By the end of the 12-hour build-up, both models have recovered toward their respective initial pressures of 100.011 bara for the Temperature model and 99.649 bara for the Compositional Thermal model, consistent with the simulation pressure during the doublet operation.

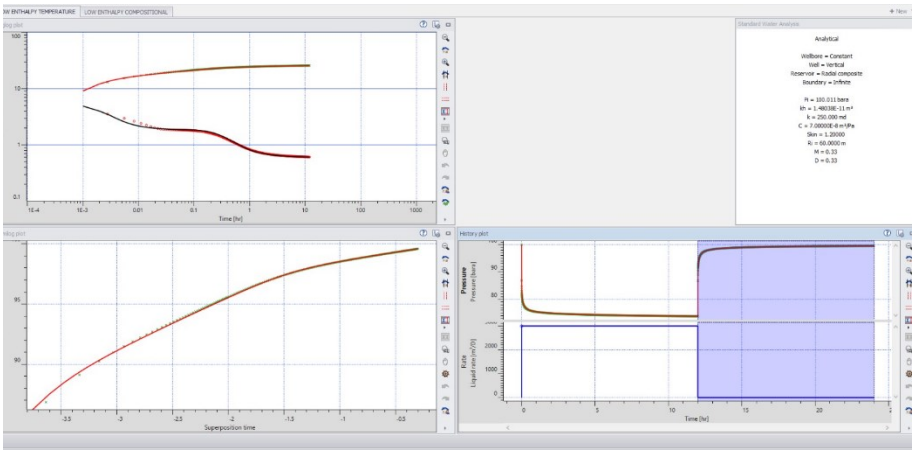

Figure 26 — Case 1 (Low-Enthalpy, 100 bara / 92°C): ***Kappa Ecrin pressure transient analysis of the well test done for the injector — Temperature model. Top-left: log-log diagnostic plot of pressure difference (ΔP) and logarithmic derivative (ΔP') versus elapsed time. Bottom-left: Horner superposition semi-log plot. Bottom-right: pressure and liquid rate history.***

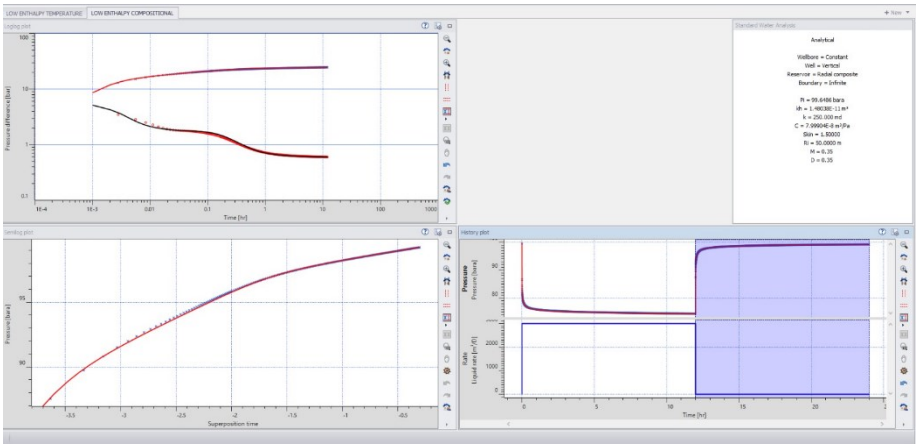

Figure 27— Case 1 (Low-Enthalpy, 100 bara / 92°C): ***Kappa Ecrin pressure transient analysis of the well test done for the injector — Compositional Thermal model. Same plot layout as Figure 26.***

Figures 26 and 27 present the Kappa radial composite analysis for the Temperature and Compositional models of Case 1. Both figures share the same diagnostic topology: wellbore storage at early time, a derivative plateau from inner-zone radial flow, and a downward composite transition as the transient crosses into the more mobile warm outer zone. Since both models use identical reservoir geometry, permeability, and matching constraints, any difference between the two figures originates entirely from the distinct pressure transients each formulation produced during the 6 months doublet operation.

That difference shows up in the timing of the composite transition. The Temperature model's derivative step falls between $\Delta t \approx 0.3$ and 2 hr —

corresponding to Ri = 60.0 m. The Compositional model reaches its transition roughly 30–40% earlier in elapsed time, placing Ri at 50.0 m. The earlier transition is simply because the Compositional model's cold zone ends at 50 m, not 60 m. Both plateaus stabilize at the same derivative level (~0.08–0.09 bar), which is exactly what identical kh = 15,000 mD·m and near-identical inner-zone viscosities (0.95 cP for TEMP, 0.90 cP for COMP) at the composite boundary would predict.

The skin factors of +1.20 for the Temperature model and +1.50 for the Compositional Thermal model, are moderately positive but do not indicate near-wellbore damage. They compensate for the step-change model's inherent inability to represent the continuous viscosity gradient that exists across the thermal front, and their near-identical values confirm that this compensation works the same regardless of which formulation generated the transient.

6.2.2. Case 2 – High-Enthalpy Scenario

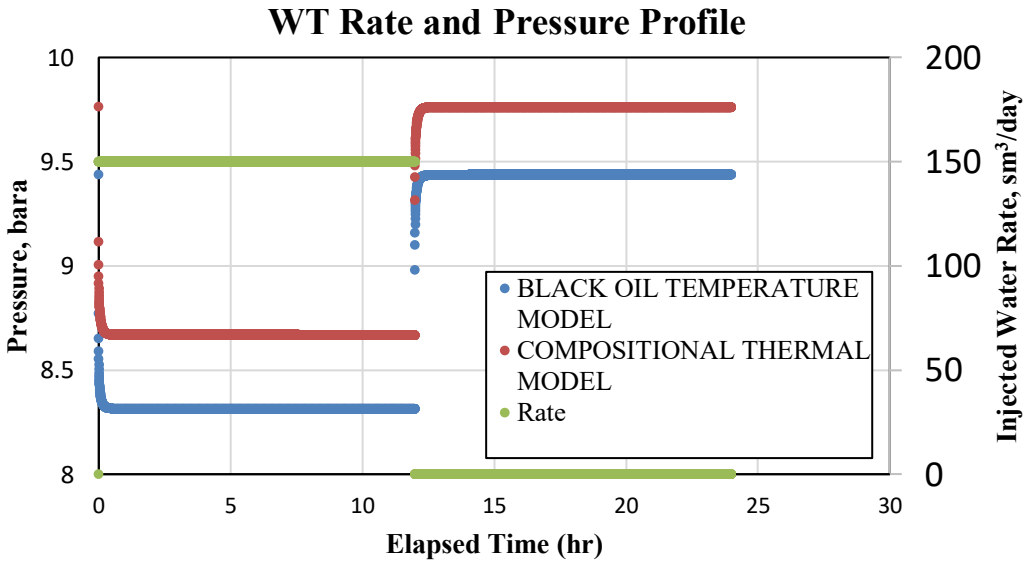

Figure 28 — Case 2 (High-Enthalpy, 10 bara / 181°C): ***Bottom-hole pressure and water rate history at the injector well (INJ) during the 12-hour production / 12-hour shut-in well test.***

The pressure drop during the 12-hour drawdown is small — only 0.3–0.6 bara — reflecting the extreme mobility of the steam outer zone at 10 bara, which absorbs the production disturbance with almost no resistance. After shut-in, both models recover quickly toward their respective equilibrium pressures. The Temperature model builds up to Pi ≈ 9.44 bara and the Compositional model to Pi ≈ 9.76 bara. But the ordering reverses compared to Case 1: there Pi_TEMP > Pi_COMP, but here Pi_COMP > Pi_TEMP by about 0.32 bara.

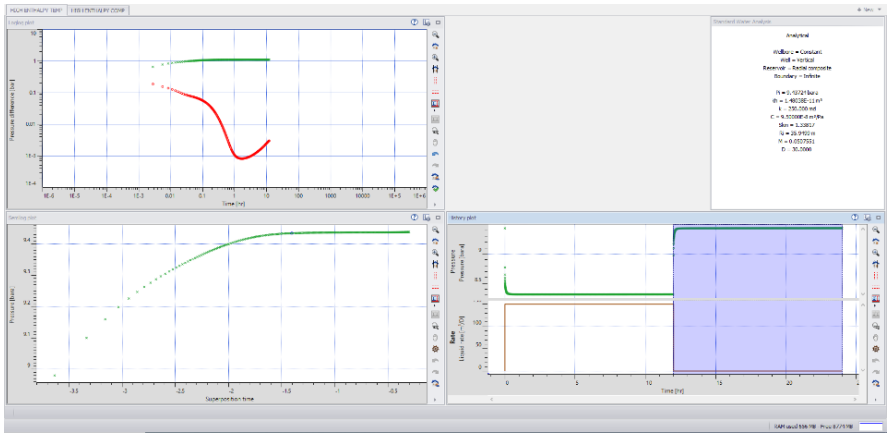

Figure 29 — Case 2 (High Enthalpy, 10 bara / 181°C): ***Kappa Ecrin pressure transient analysis of the well test done for the injector — Temperature model. Same plot layout as Figure 26.***

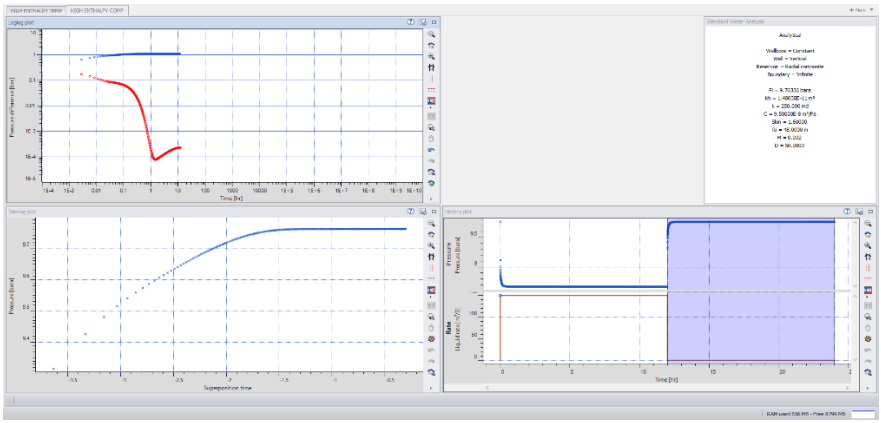

Figure 30 — Case 2 (High Enthalpy, 10 bara / 181°C): ***Kappa Ecrin pressure transient analysis of the well test done for the injector — Compositional Thermal model. Same plot layout as Figure 26.***

Figures 29 and 30 show the Kappa plots for the Case 2 Temperature model and Compositional Thermal model build-up pressure transient analysis during the well tests done after ten years of doublet operation.

Both plots reproduce the same broad three-stage shape seen in Case 1 — wellbore storage at early time, an inner-zone derivative plateau, and a downward composite transition — but with two crucial differences in character. The transition itself is far more abrupt, where Case 1 showed a moderate downward step governed by M ≈ 0.33-0.35, Case 2 produces a near-collapse of the derivative driven by the extreme viscosity contrast between cold liquid water (μ ≈ 1.001 cP) and superheated steam (μ_steam ≈ 0.015 cP). And after the transition, the late-time derivative rises rather than settling into a second stable plateau, a behavior that the conventional two-zone composite model cannot reproduce.

The early plateau, which is the most interpretable feature of both figures, corresponds to inner-zone radial flow through the cold liquid water bank around the injector. The plateau level is governed by $\frac{kh}{\mu_{inner}}$ and is consistent with $\mu_{inner} \approx$ 1.001 cP at 20°C — the injection temperature — in exact agreement with the IAPWS-08 viscosity of cold water. This first stabilization is the most reliable feature of the Case 2 well test: it correctly identifies that the wellbore block is fully occupied by cold liquid. Both models produce an identical plateau level, as expected from the shared viscosity values.

The transition from the inner-zone plateau toward the steam outer-zone response begins at elapsed times corresponding to the pressure transient reaching the cold-front boundary. The Kappa-fitted composite radius is 36 m for the Temperature model and 48 m for the Compositional Thermal model, against simulated cold-zone radii of 50 m and 60 m respectively (Figure 18b). The interpretation nevertheless remains consistent with the simulation in order of magnitude and preserves the ordering between the two formulations (COMP > TEMP). Due to the absence of the second stabilization, unique estimation of mobility and storativity ratio is impossible.

6.2.3. Comparison between Well Test Scenarios

The well test results from Case 1 and Case 2 differ not only quantitatively but in character, reflecting the fundamentally different thermodynamic regimes of the two scenarios.

The most obvious difference is signal magnitude. In Case 1, producing at 3,000 sm^3/day from the liquid-dominated reservoir generates a drawdown of approximately 26 bara. In Case 2 where the steam is being produced at a rate of 150 sm^3/day a pressure drawdown of only 0.3–0.6 bara is obtained, approximately 40 times smaller for a 20-fold reduction in rate which is attached to mobility contrast. Steam at 181°C and 10 bara is nearly frictionless to flow compared to warm liquid water: k/μ_steam = 16,667 mD/cP in Case 2 against k/μ_warm water = 789 mD/cP in Case 1, a factor of roughly twenty.

The two cases also look qualitatively different on the log-log diagnostic plot. In Case 1, the transition from inner-zone to outer-zone is a valley-shaped downward step governed by M ≈ 0.33–0.35, meaning the transition from the cold inner zone to the warm outer reservoir produces a moderate downward step — roughly a two-to-threefold mobility increase at the composite boundary. Both stabilization levels are clearly detectable. Consequently, in Case 1, the pressure transients from both

formulations are clean enough that Kappa has no difficulty fitting them with a standard radial composite model and the match is exact in both cases.

On the other hand, Case 2 acts differently. The first stabilization is there and readable, and the transition away from it is visible too, but after that, the derivative does something that neither model predicts cleanly. Rather than settling into a second plateau, it climbs, and it does so along a different path in each formulation. That divergence between the two models after the transition makes any attempt at a conventional composite interpretation unreliable. Such behavior may be due to the extreme viscosity (M = 0.015) and compressibility (D ~ 20) contrast between cold liquid water and superheated steam; however, possible boundaries effects, incomplete equilibration before the test and phase exchange can also have an impact. A deep study of this behavior was beyond the scope of the present study and therefore merits further investigation.

Table 7 summarizes all matched and measured parameters across both cases.

Table 7 — Summary of all matched and measured parameters across both cases and both formulations

Parameter	Case 1 TEMP	Case 1 COMP	Case 2 TEMP	Case 2 COMP
Ri (m)	**60.0**	**50.0**	**36.0**	**48.0**
M	0.33	0.35	-	-
D	0.33 = M	0.35 = M	-	-
Pi (bara)	100.011	99.649	~9.44	~9.76
Skin	+1.20	+1.50	—	—

Chapter 7 - Conclusions

This thesis investigated the applicability of injection-well pressure transient analysis as a monitoring tool for tracking cold-front propagation in geothermal doublets. Numerical simulations were performed using the Temperature (TEMP) and Compositional Thermal (THERMAL) formulations available in tNavigator®, and the resulting pressure responses were interpreted with a radial composite model in Saphir NL. The objective was to evaluate both the capability of well testing to

estimate the extent of the cooled zone around the injector and the impact of the selected thermal formulation on thermal-front prediction.

The results obtained for the low-enthalpy liquid-dominated reservoir demonstrate that injection-well pressure transient analysis can provide a reliable estimate of the cold-water bank extension. The pressure-derivative response is characterized by the behavior of a radial composite system, and the composite radii recovered from Saphir showed an agreement with the thermal-front radii measured directly from the numerical simulations. This confirms that, when the viscosity of the cooled zone is properly constrained to injection temperature conditions, the radial composite interpretation provides a meaningful approximation of the thermal front geometry.

Despite the single-phase nature of the low-enthalpy case, significant differences were observed between the two thermal formulations. After six months of operation, the predicted thermal-front extension differed by approximately 20%.

The root cause traces back to how each formulation handles formation volume factor, density, and compressibility as temperature changes, properties that the Temperature model anchors at a fixed reference condition while the Compositional model recomputes dynamically for each cell. Even in a single-phase liquid system with no phase transitions, that difference is enough to shift the predicted cold-front position by a non-negligible margin.

Moving to the high-enthalpy vapor-dominated case, the gap between the two formulations widened further — which was not surprising given what the Temperature model is fundamentally incapable of doing. Steam condensation at the advancing cold front, the latent heat released in the process, and the phase-equilibrium dynamics that govern how the two-phase boundary evolves are all outside what a black-oil thermal framework can represent. The Compositional model, computing phase state and fluid properties dynamically, gave a physically sounder picture of how the cold zone develops in a steam reservoir.

The high-enthalpy case also produced something the standard radial composite framework could not account for. After the first derivative stabilization, the plateau associated with the cooled inner zone, the derivative rose again in a way that does not match a closed-boundary signature. What drives that rise is not entirely clear: phase transitions at the cold-front boundary, the extreme mobility contrast between cold liquid water and superheated steam, large compressibility differences between the two zones, or some combination of all three are plausible contributors. Resolving it properly would require a detailed investigation that was beyond the scope of the present work and remains an important subject for future research.

Taken together, the results make a reasonably clear case that injector well testing can work as a cold-front monitoring tool in geothermal doublets, at least where the reservoir is liquid-dominated and the physics stays tractable. At the same time, the results show that thermal-front numerical predictions are highly sensitive to the underlying thermodynamic formulation. Consequently, careful selection of the simulation model is essential when estimating thermal breakthrough and the long-term performance of geothermal doublets. These findings provide practical guidance for geothermal reservoir characterization and well-test interpretation.

Appendix A: keywords, options, and capabilities for the Black Oil Temperature option vs. Compositional Thermal model

This appendix provides a complete side-by-side comparison of the tNavigator® (*tNavigator® Technical Reference Manual*, 2024) keywords, options, and capabilities for the Black Oil + Temperature model (TEMP) and the Compositional Thermal model (COMP) formulations used in this study. The tables are included for reference and reproducibility; the physical basis for the selection of each formulation is discussed in Chapter 3.

Phases	**Black Oil+Temperature model**	**Compositional+Thermal Model**
Oil	B_o and R_s $\rho_0 = \frac{\rho_{O,ST} + R_s \rho_{G,SC}}{B_o}$	$\rho_{k,0} = \frac{\rho_{k,ref}}{(1 - c_{k,p}(P - P_{ref}))(1 + c_{k,T}(T - T_{ref}))}$
Standard/Thermal Water	-	○ Pure, single component: **Polynomial + exponential pressure compressibility** term: **WATDENT** $\rho_W = \frac{A_0 + A_1 T + A_2 T^2 + A_3 T^3 + A_4 T^4 + A_5 T^5}{1 + A_6 T} * e^{c_{w,P}(P - A_7)}$
Multicomponent Water	Constant + Compressibility PVTW	CO2STORE BRINE ○ Rowe-Chou Method: density function of: T, P, salt-AQUDEN ○ Multicomponent water with dissolved Gases and Salts: **Ezrokhi's method**:

		$\log \rho_W = \log \rho_0 (P,T) + \sum A_i w_i$ Where temperature-dependent coefficient for each specific dissolved component: $A_i = a_{0,i} + a_{1,i}T + a_{2,i}T^2$ (density adjustments function of dissolved components like NaCl, CO2-DENAQA)
Gas	• Standing's Correlation: $PV = znRT$ • Hall-Yarborough Correlation: $B_g = 0.02827 \frac{z*T}{P}$ • Tubular: PVTG (wet gas), PVTD (dry gas)	• EOS: $P = \frac{RT}{v-b} - \frac{a}{(v+m_1 b)(v+m_2 b)}$ PR, SRK, RK, MPR, **GERG-2008**

	Black Oil + Temperature	**Compositional + Thermal**
Manual reference	2.31.	4.
Tutorials	SIM6.2. How to Use Temperature.	○ SIM1.9. How to Use Thermal ○ MD 3.3. How to Create Geothermal Model
Multi-component water	No	YES COMPW ○ KVCRWAT

Main keywords	TEMPR TEMP	THERMAL
Phases	Water, Oil, Gas	Water, Oil, Gas, Solid
Phase changes (i.e. water vaporization and water condensation)	NO	YES (Water vaporization, Gas condensation, Oil evaporation, Combustion, Carbonization) TABDIMSS
Enthalpy and Internal Energy	Fluid enthalpy is independent of component composition	YES, depends on P, T, and Composition SPECHA SPECHB SPECHG SPECHH HEATVAP
Thermal Conductivity of Rock	THCONR THCROCK	THCROCK
Thermal Conductivity of phases	THCWATER THCGAS THCOIL THSOLID	THCOIL THCWATER THCGAS THCSOLID THCONMIX THCOCOEF THCGCOEF THCWOEF THCRCOEF
Thermal Convection	YES, CONVECTION ENTHALPY FLOW	FULLY COUPLED: Energy conservation is solved simultaneously with the fluid flow equation
Thermal Exchange with rock	THCONR ROCKCONT	THCROCK THCONR ROCKPROP HLOSSPROP HEATCR HEATCRT
Fluid viscosity changes with temperature	WATVISCT OILVISCT VISCREF	OILVISCT OILVISCC GASVISCF GASVISCT WATVISCF STEVISCF LBCCOEF

Fluid density changes with temperature	Via PVT props or thermal expansion in Geomechanics	WATDENT DENSITY THERMEX1 THERMEX2 PVTWSALT (brine)
Solid density changes with temperature	-	SOLID SDREF ICE
Phase Specific Heat Capacity (Enthalpy) changes with temperature	SPECHEAT	SPECHA SPECHB SPECHC SPECHD SPECHG SPECHH SPECHW1 SPECHW2 SPECHS SPECHT HEATVAPS
Rock Heat Capacity changes with temperature	SPECROCK THCONR	HEATCR HEATCRT HEATTCR ROCKCP_SHL
Relative Permeability changes with temperature (End-Point scaling)	NO	ENPTVT ENKRVT ENPTVTEXT
Formation volume factor changes with temperature	Implicit in PVT tables PVCO PVDO PVTO PVDG PVTG PVTW	Calculated via EOS ibo ibg ibw
Fluid saturation changes with temperature	Result of flow and pressure changes	Result of Thermodynamic Equilibrium (Flash) calculated at T
Permeability changes with temperature	ROCKCONT TRMTEMP	ENPTVT ENKRVT ENPTVTEXT PERMSHALE

EOS	TCRIT PCRIT CNAMES AQCOEF BICAQ1 BICAQ2 BICAQ3	EOS (PR, SRK, GERG-2008) TCRIT PCRIT CNAMES ZCRIT PARACHOR
Reservoir temperature with depth	RTEMPVD RTEMPA	TEMPVD RTEMP
Heat energy injection/production rate	WTIRHEA WTPRHEA	WTIRHEA WTPRHEA HEATER WHEATER
Injection Temperature	WTEMP WTEMPDEF	WINJTEMP WINJOIL WINJGAS

References

Axelsson, G., 2013. Tracer tests in geothermal resource management. EPJ Web of Conferences 50, 02001. https://doi.org/10.1051/epjconf/20135002001

Bahadori, A., 2017. Fluid phase behavior for conventional and unconventional oil and gas reservoirs. Gulf Professional Publishing, Amsterdam, [Netherlands].

Bejan, Adrian, N., Donald A., 2006. Convection in Porous Media, Third Edition. ed. Springer Science+Business Media, New York, NY.

Bertani, R., 2016. Geothermal power generation in the world 2010–2014 update report. Geothermics 60, 31–43. https://doi.org/10.1016/j.geothermics.2015.11.003

Bödvarsson, G.S., Tsang, C.F., 1982. Injection and Thermal Breakthrough in Fractured Geothermal Reservoirs. J. Geophys. Res. 87, 1031–1048. https://doi.org/10.1029/JB087iB02p01031

Çengel, Y.A., 2003. Heat transfer: a practical approach, 2nd ed. ed. McGraw-Hill, Boston.

Croucher, A.E., O'Sullivan, M.J., 2008. Application of the computer code TOUGH2 to the simulation of supercritical conditions in geothermal systems. Geothermics 37, 622–634. https://doi.org/10.1016/j.geothermics.2008.03.005

Della Vedova, B., Vecellio, C., Bellani, S., Tinivella, U., 2008. Thermal modelling of the Larderello geothermal field (Tuscany, Italy). Int J Earth Sci (Geol Rundsch) 97, 317–332. https://doi.org/10.1007/s00531-007-0249-0

Ebigbo, A., Niederau, J., Marquart, G., Dini, I., Thorwart, M., Rabbel, W., Pechnig, R., Bertani, R., Clauser, C., 2016. Influence of depth, temperature, and structure of a crustal heat source on the geothermal reservoirs of Tuscany: numerical modelling and sensitivity study. Geotherm Energy 4, 5. https://doi.org/10.1186/s40517-016-0047-7

Farzaneh-Gord, M., Rahbari, H.R., Mohseni-Gharesafa, B., Toikka, A., Zvereva, I., 2021. Accurate determination of natural gas compressibility factor by measuring temperature, pressure and Joule-Thomson coefficient: Artificial neural network approach. Journal of Petroleum Science and Engineering 202, 108427. https://doi.org/10.1016/j.petrol.2021.108427

Fokker, P.A., Salina Borello, E., Viberti, D., Verga, F., Van Wees, J.-D., 2021. Pulse Testing for Monitoring the Thermal Front in Aquifer Thermal Energy Storage. Geothermics 89, 101942. https://doi.org/10.1016/j.geothermics.2020.101942

Garg, S.K., Pritchett, J.W., 1990. Cold water injection into single- and two-phase geothermal reservoirs. Water Resources Research 26, 331–338. https://doi.org/10.1029/WR026i002p00331

HE, J., 2017. FINITE DIFFERENCE SIMULATION OF THESTOKES-BRINKMANEQUATION FORTRANSIENTFLOWINNATURALLYFRACTUREDCARBONATE KARST RESERVOIRS (Dissertation). Texas A&M University.

Huber, M.L., Perkins, R.A., Laesecke, A., Friend, D.G., Sengers, J.V., Assael, M.J., Metaxa, I.N., Vogel, E., Mareš, R., Miyagawa, K., 2009. New International

Formulation for the Viscosity of H2O. Journal of Physical and Chemical Reference Data 38, 101–125. https://doi.org/10.1063/1.3088050
Kareem, L.A., 2014. Z Factor: Implicit Correlation, Convergence Problem and Pseudo-Reduced Compressibility, in: SPE Nigeria Annual International Conference and Exhibition. Presented at the SPE Nigeria Annual International Conference and Exhibition, SPE, Lagos, Nigeria, p. SPE-172373-MS. https://doi.org/10.2118/172373-MS
Khait, M., Voskov, D., 2018. Operator-based linearization for efficient modeling of geothermal processes. Geothermics 74, 7–18. https://doi.org/10.1016/j.geothermics.2018.01.012
Kunz, O., Wagner, W., 2012. The GERG-2008 Wide-Range Equation of State for Natural Gases and Other Mixtures: An Expansion of GERG-2004. J. Chem. Eng. Data 57, 3032–3091. https://doi.org/10.1021/je300655b
Liu, H., Chen, Z., Shen, L., Guo, X., Ji, D., 2020. Well modelling methods in thermal reservoir simulation. Oil Gas Sci. Technol. – Rev. IFP Energies nouvelles 75, 63. https://doi.org/10.2516/ogst/2020058
Lund, J.W., Toth, A.N., 2021. Direct utilization of geothermal energy 2020 worldwide review. Geothermics 90, 101915. https://doi.org/10.1016/j.geothermics.2020.101915
Nkinyam, C.M., Ujah, C.O., Asadu, C.O., Kallon, D.V.V., 2025. Exploring geothermal energy as a sustainable source of energy: A systemic review. Unconventional Resources 6, 100149. https://doi.org/10.1016/j.uncres.2025.100149
Romagnoli, P., Arias, A., Barelli, A., Cei, M., Casini, M., 2010. An updated numerical model of the Larderello–Travale geothermal system, Italy. Geothermics 39, 292–313. https://doi.org/10.1016/j.geothermics.2010.09.010
Satman, A., Mauricio, E., Tang, R.W.-K., Ramey, H.J., 1980. An Analytical Study of Transient Flow in Systems with Radial Discontinuities, in: SPE Annual Technical Conference and Exhibition. Presented at the SPE Annual Technical Conference and Exhibition, SPE, Dallas, Texas, p. SPE-9399-MS. https://doi.org/10.2118/9399-MS
Sbai, M.A., Larabi, A., 2023. Analyzing the relationship between doublet lifetime and thermal breakthrough at the Dogger geothermal exploitation site in the Paris basin using a coupled mixed-hybrid finite element model. Geothermics 114, 102795. https://doi.org/10.1016/j.geothermics.2023.102795
Schölderle, F., Lipus, M., Pfrang, D., Reinsch, T., Haberer, S., Einsiedl, F., Zosseder, K., 2021. Monitoring cold water injections for reservoir characterization using a permanent fiber optic installation in a geothermal production well in the Southern German Molasse Basin. Geotherm Energy 9, 21. https://doi.org/10.1186/s40517-021-00204-0
Stopa, J., Wojnarowski, P., 2006. Analytical model of cold water front movement in a geothermal reservoir. Geothermics 35, 59–69. https://doi.org/10.1016/j.geothermics.2005.11.002
tNavigator® Technical Reference Manual (Software Manual No. Version 25.3), 2024. . Rock Flow Dynamics, London.
USDOE Office of Energy Efficiency and Renewable Energy (EERE), Idaho National Laboratory (INL), Idaho Falls, ID (United States), Plummer, M., Mattson, E., Palmer, C., Redden, G., Elias, G., Hull, L., 2011. Advancing Reactive Tracer Methods for Measurement of Thermal Evolution in

Geothermal Reservoirs (Final Report) (No. INL/EXT--11-22632, 1033883). https://doi.org/10.2172/1033883

Wagner, W., Cooper, J.R., Dittmann, A., Kijima, J., Kretzschmar, H.-J., Kruse, A., Mareš, R., Oguchi, K., Sato, H., Stö cker, I., Šifner, O., Takaishi, Y., Tanishita, I., Trü benbach, J., Willkommen, Th., 2000. The IAPWS Industrial Formulation 1997 for the Thermodynamic Properties of Water and Steam. Journal of Engineering for Gas Turbines and Power 122, 150–184. https://doi.org/10.1115/1.483186

Young, L.C., 2022. Compositional Reservoir Simulation: A Review. SPE Journal 27, 2746–2792. https://doi.org/10.2118/208610-PA

Zaydullin, R., 2014. COMPOSITIONAL SPACE PARAMETERIZATION METHODS FOR THERMAL-COMPOSITIONAL SIMULATION (Dissertation). STANFORD UNIVERSITY.